Neutron Scattering Investigations on the Unusual Phase Behavior of Water

by

Yang Zhang

B.S., University of Science and Technology of China (2004)

Submitted to the Department of Nuclear Science and Engineering
in partial fulfillment of the requirements for the degree of

Doctor of Philosophy

at the

MASSACHUSETTS INSTITUTE OF TECHNOLOGY

August 2010

Author .....
Department of Nuclear Science and Engineering
August 25, 2010

Certified by .....
Sow-Hsin Chen
Professor of Nuclear Science and Engineering
Thesis Supervisor

Certified by .....
Sidney Yip
Professor of Nuclear Science and Engineering
and Materials Science and Engineering
Thesis Reader

Accepted by .....
Mujid S. Kazimi
Professor of Nuclear Science and Engineering
and Mechanical Engineering
Chairman, Department Committee on Graduate Students

Neutron Scattering Investigations on the Unusual Phase Behavior of Water

by

Yang Zhang

Submitted to the Department of Nuclear Science and Engineering
on August 25, 2010, in partial fulfillment of the
requirements for the degree of
Doctor of Philosophy

Abstract

Water is the most ubiquitous substance on earth, and is essential to sustain all known forms of life. However, despite centuries of research, a coherent picture of the unusual phase behavior of water is so far lacking. The most promising theory under scrutiny relies on the hypothetical existence of a liquid-liquid phase transition and an associated liquid-liquid critical point hidden in the region of supercooled temperatures and elevated pressures, where bulk water does not exist in liquid state. Therefore it is a grand experimental challenge to investigate the properties of water, both thermodynamic and dynamic, in the relative region of the phase diagram.

A combination of neutron triple-axis spectrometer and small-angle neutron scattering instrument are used to measure the density of water confined in a nanoporous silica matrix MCM-41-S in a Temperature-Pressure range inaccessible for the bulk (300–130 K and 1–2900 bar), namely, the equation of state $\rho(T, P)$. The measured isobaric density profiles clearly show a change of behavior around 1500 bar. This experiment provides the most direct evidence supporting the existence of a liquid-liquid critical point in such confined water. The experimental result further implies that the nature of the liquid-liquid critical point of water might be of a tricritical type. Moreover, the reported density data of confined water under extreme conditions are valuable for the vast communities in biological, geological and planetary sciences.

Parallel to the density measurement, the dynamics of water in confined geometry, such as aged cement paste and the vicinity of protein surfaces, are also investigated using a variety of quasi-elastic and inelastic neutron scattering spectrometers. A wide range of pre-glass-transition phenomena, such as dynamic crossover, dynamic heterogeneity and boson peak, are observed above the conventional glass-transition temperature. Possible explanations are discussed in the frameworks of the liquid-liquid critical point scenario of water and the extended mode-coupling theory.

Computer simulations are frequently exploited to achieve a unified interpretation. These new findings of confined water may provide new insights to the research on glassy systems of multi-scales as well as innumerable examples in soft condensed matters, where randomness and cooperativity are common and intrinsic.

Thesis Supervisor: Sow-Hsin Chen
Title: Professor of Nuclear Science and Engineering

Thesis Reader: Sidney Yip
Title: Professor of Nuclear Science and Engineering
and Materials Science and Engineering

Acknowledgments

First and foremost, I feel very privileged to have worked with my thesis supervisor Professor Sow-Hsin Chen, who believed in me, inspired me, and guided me to the field of neutron/X-ray scattering and water science. His enthusiasm for science has encouraged and will keep encouraging me for the rest of my life. Also, I would like to express my sincere gratitude to my thesis reader Professor Sidney Yip, who always supported me and offered me invaluable advices.

Special thanks to my thesis committee members: Professor H Eugene Stanley, Professor Pablo G Debenedetti, Professor David Chandler, and Professor Bilge Yildiz. Their exceptional intuitions, profound insights, constructive comments influenced me enormously throughout the past five years.

I owe a great debt to my collaborators and fellow students for their substantial assistance in sample preparations, experiments, and all other possible ways. They are Prof P Baglioni, E Fratini, F Ridi (U of Florence); Prof C-Y Mou, K-H Liu, C-C Chen, C-W Yen (NTU); Prof F Mallamace (U of Messina); M Lagi, C-S Tsao, J Wu (MIT); S-H Chong (Inst for Mol Sci); Prof M Medina-Noyola (U Autonoma San Luis Potosi); X Li, L Liu (RPI); Prof P Tartaglia, Prof F Sciortino (U of Rome I); M Broccio (CMU); A Faraone, Y Liu, WA Kamitakahara, JB Leao, S Chang, JRD Copley, Y Qiu, C Brown, M Tyagi, T Jenkins, V Garcia-Sakai, P Butler, J Krzywon, T Udovic, DA Neumann, R Dimeo (NIST); W-R Chen, D Liu, X Chu, E Mamontov, K Herwig, M Hagen, AI Kolesnikov, AP Sokolov, T Egami, DAA Myles, KC Littrell, Y Melnichenko, G Smith, S Nagler, I Anderson (ORNL); DG Wonzniak, P Thiyagarajan, C-K Loong, V Pingali, A Alatas, A Said, BM Leu, E Alp, Y Shvydko, H Sinn (ANL). My acknowledgment also goes to the countless others at MIT, NIST, ORNL and ANL, who have helped me. All of your efforts made the work in this thesis possible.

Finally, I dedicate this thesis to my wife Xiaojun Yang, my father Zhanwu Zhang and my mother Liping Yang. I love you.

THIS PAGE INTENTIONALLY LEFT BLANK

Contents

List of Figures

THIS PAGE INTENTIONALLY LEFT BLANK

List of Tables

THIS PAGE INTENTIONALLY LEFT BLANK

Chapter 1

Introduction

If there is magic on this planet, it is contained in water.

— Loren Eiseley

1.1 The anomalous properties of water

What substance could possibly more important than water? Indeed, water is vital to life; water sculpts the geological environments; water is the most frequently handled materials in industry; the list goes on and on. For these reasons, water is often believed to possess spiritual powers in almost every religion and philosophy. Water's unique symbolic significance again attests to its essential role in our lives[11, 113, 5, 3, 47, 46].

The scientific thought on water has been long[15]. Water is used as scientific standards in many cases. For example, the Kelvin temperature scale of the SI system is defined such that the triple point of water is exactly 273.16 K. And the gram is defined as the weight of one cubic centimeter of water at the temperature of melting ice at ambient pressure. However, it is embarrassing to admit that despite centuries of intensive research, we still don't have a satisfying theory to coherently explain the properties of water so far[13, 100].

Water behaves quite differently from other liquids in many ways. More than 60 anomalies[12, 52] of water have been found, among which the most well-known one is probably that water expands when it freezes into ice. Otherwise, people will not be able to skate on a lake in winter. However, a coherent explanation of all of the anomalies still does not exist[26, 100, 113, 142]. Furthermore, the newly-discovered counterintuitive properties make the topic even more interesting, some of which will be shown in this thesis.

1.2 Supercooling and "no man's land"

The anomalous properties of water become amplified in the supercooled region[159]. Supercooling is the process of lowering the temperature of a liquid below its melting/freezing temperature while maintaining the liquid state. The supercooling process can be achieved by cooling very pure liquid. Because of the lack of nucleus, the liquid is just difficult to crystallize. In a similar way, a liquid can also be superheated above its boiling temperature. Both supercooled and superheated liquids are metastable[45]. They may transfer to the corresponding stable states in the presence of nucleation sites or perturbations.

In the supercooled region, the three thermodynamic response functions, the isothermal compressibility κ_T, the isobaric thermal expansion coefficient α, and the specific heat capacity at constant pressure c_P deviate from those of other liquids dramatically. They seem to become diverge at a singularity temperature $T_s \approx 228$ K[5]. However, this temperature is already below the homogeneous nucleation temperature of water at ambient pressure, so liquid water is difficult to maintain.

If the cooling process is fast enough, say in the order of 10^6 K/s, water can be immediately brought to its amorphous or glassy state. The actual glass transition temperature T_g of water is hard to estimate and is still under debate. Despite of that, the study of glass transition in general is a grand challenge for statistical physics

due to its non-equilibrium, non-ergodic, and disordered natures[8, 49, 68, 50, 145]. A lot of theoretical and experimental efforts have been devoted into the research on the glasses[48, 4, 88, 75]. When the glassy water is heated up about 150 K, it will form ice again. So between this temperature and the homogeneous nucleation temperature, there is a region, often called "no man's land", where bulk water does not exist[106, 101].

The most promising theory of water under scrutiny relies on the hypothesis of the existence of a liquid-liquid phase transition and an associated liquid-liquid critical point hidden in the "no man's land"[113] at deeply supercooled temperatures and elevated pressures[126, 63, 123]. Other possible competing theories under examination include the "singularity-free scenario"[130] and the "critical point-free scenario"[9]. The central question, still waiting for an experimental answer, is whether or not a second critical point exists in the "no man's land" of water. Therefore it is a grand experimental challenge to investigate the properties of water, both thermodynamic and dynamic, in the relevant region of the phase diagram where the peculiar properties of water may originate[141, 26, 13, 24, 25, 100, 92].

One of the methods to suppress the homogeneous nucleation process is to use confinement[127]. Thus, in the restricted geometry, the ice formation is inhibited, which allows us to enter the "no-man's land" to study the properties of water in a liquid phase. In fact, confined water plays a fundamental role in many kinds of biological, geological, and industrial processes, where the water-substrate interaction, hydrophilic or hydrophobic, together with the geometry of the confinement modifies the formation of the random hydrogen bond network and thus the overall energy landscape of the system.

1.3 Neutron scattering and computer simulations

Neutron scattering technique provides a collection of powerful instruments for material characterization[34, 51, 23, 120]. It is especially useful for the study of water because of the exceptionally large incoherent cross section of hydrogen and the capability of varying contrast with different isotopes. Nowadays, high-flux neutrons are readily produced at a nuclear reactor or an accelerator-based spallation source. A combination of various elastic, inelastic and quasi-elastic neutron scattering instruments allow simultaneous measurements of the structure and dynamics at different scales.

On the other hand, modern neutron scattering technique basically measures only the density-density correlation function and quantities that can be deduced from it. In a way, the measurements involve integrations over the microscopic motions and are consequently not sensitive to the details. Computer simulations are also frequently exploited to explore the physical quantities hardly accessible by experiments and to achieve a unified interpretation. However, it must be pointed out that computer simulation is always limited by the computation power, while in many experiments some physical quantities can be measured with high accuracy, in principle, allowing us to examine the detailed information of the investigated system. The combination of experimental technique and computer simulations is becoming a common way to conduct any type of research.

1.4 Overview of the thesis

This thesis is consisted of four chapters. The current Chapter 1 is a general introduction of the scientific merits of water science and the methods used to tackle this problem. The main body of the thesis has two parts: the equation of state of confined water $\rho(P,T)$ discussed in Chapter 2, and the pre-glass-transition phenomena of confined water discussed in Chapter 3. In each of these chapters, relevant sample

descriptions, experimental techniques and data analysis are explained. Most of the contents are based on my publications in the past five years, listed in Appendix A. But more efforts are paid to elucidate the essential logic among those publications. The last Chapter 4 surveys the research on water in a broader sense.

THIS PAGE INTENTIONALLY LEFT BLANK

Chapter 2

Equation of state: thermodynamics

Zeroth: "You must play the game."

First: "You can't win."

Second: "You can't break even."

Third: "You can't quit the game."

— Charles P Snow

2.1 Density and phase transitions

2.1.1 Thermodynamic state functions and response functions

The most convincing method to study phase transitions and critical phenomena[143] is probably through the equation of state. An equation of state is a relation between the *thermodynamic state functions*[1], which are not totally independent. Oftentimes, the thermodynamic state functions are discussed in the form of conjugate pairs of an

[1]The *thermodynamic state functions* are often abbreviated as the state functions or state variables. The word "thermodynamic" is intentionally put in front of it here to distinguish the other class of *dynamic state functions* discussed in Chapter 4. In the following, the abbreviated form of the term is often used. The authors should able to easily identify the meaning of the term from the context.

intensive quantity (generalized force) and an extensive quantity (generalized displacement) whose product has the dimension of energy, such as pressure P and volume V, temperature T and entropy S, chemical potential μ and particle number N, magnetic field H and magnetization M[29]. There is no general rule to determine the minimum number of state functions sufficient to fully describe a thermodynamic state. However, for many classical cases, when the particle number is fixed and there is no magnetic field applied, or the effect of those control variables are not concerned, it is readily to only consider the following four thermodynamic state functions: pressure P, temperature T, volume V and entropy S. Once the physics is understood in this simplified situation, it could be easily generalized to more complicated situations when there are more control variables.

Normally, the equations of state between P, T, V, S are expressed as

$$V = V(P,T) \tag{2.1}$$

$$S = S(P,T) \tag{2.2}$$

because pressure P and temperature T can be controlled experimentally. When these eqations of state are known precisely, it is readily to calculate the three standard *thermodynamic response functions*[2] by taking the partial derivatives with respect to P and T respectively[74, 28, 29, 143].

1. Isothermal compressibility

$$\kappa_T = -\frac{1}{V}\left(\frac{\partial V}{\partial P}\right)_T = -\frac{1}{V}\frac{\partial^2 G}{\partial P^2} \tag{2.3}$$

[2]Similar to Footnote 2.1.1, the *thermodynamic response functions* are often abbreviated as the response functions. The word "thermodynamic" is intentionally put in front of it here to distinguish the other class of *dynamic response functions* discussed in Chapter 4. In the following, the abbreviated form of the term is often used. The authors should able to easily identify the meaning of the term from the context.

2. Isobaric thermal expansion coefficient

$$\alpha = \frac{1}{V}\left(\frac{\partial V}{\partial T}\right)_P = -\frac{1}{V}\left(\frac{\partial S}{\partial P}\right)_T = \frac{1}{V}\frac{\partial^2 G}{\partial P \partial T} \tag{2.4}$$

3. Specific heat capacity at constant pressure

$$c_P = \frac{T}{N}\left(\frac{\partial S}{\partial T}\right)_P = -\frac{T}{N}\frac{\partial^2 G}{\partial T^2} \tag{2.5}$$

Other commonly-used response functions include

1. Adiabatic compressibility

$$\kappa_S = -\frac{1}{V}\left(\frac{\partial V}{\partial P}\right)_S \tag{2.6}$$

2. Specific heat capacity at constant volume

$$c_V = \frac{T}{N}\left(\frac{\partial S}{\partial T}\right)_V \tag{2.7}$$

They can be determined from the above-mentioned three standard response functions using the following relations[10]

1. Compressibility:

$$\kappa_T - \kappa_S = \frac{TV\alpha^2}{Nc_P} \tag{2.8}$$

2. Specific heat capacity:

$$c_P - c_V = \frac{TV\alpha^2}{N\kappa_T} \tag{2.9}$$

2.1.2 Thermodynamic fluctuations and phase transitions

For a single component system, the three standard response functions are sufficient to describe the thermodynamic behaviors of the system. They are all the possible second order derivatives of the free enthalpy or Gibbs free energy G, which takes minimum

value at fixed pressure P and temperature T. Each of these response functions is associated with a microscopic fluctuation[46, 47]

$$\langle (\delta V)^2 \rangle = k_B T V \kappa_T \tag{2.10}$$

$$\langle \delta V \delta S \rangle = k_B T V \alpha \tag{2.11}$$

$$\langle (\delta S)^2 \rangle = k_B N c_P \tag{2.12}$$

where k_B is the Boltzmann constant, δ denotes the fluctuation in a random variable A about its expectation

$$\delta A = A - \langle A \rangle \tag{2.13}$$

Specifically, the isothermal compressibility reflects the volume fluctuation; the specific heat at constant pressure reflects the entropy fluctuation; and the isothermal expansion reflects the cross-correlation between volume and entropy fluctuations. On approaching a critical point, the three response functions will grow in the forms of power-law dependence on the correlation length ξ and eventually diverge at the critical point. This is because the fluctuations between different phases becomes larger and larger and the correlation length becomes infinite at the critical point. It is surprising that for a large class of very different systems the exponents of the power-laws take the same value. The critical exponents can be calculated using the renormalization group, which is intimately related to the scale invariance or self-similarity of the system. This intriguing phenomenon is usually called the *universality*[143].

Phase transitions are often caused the broken of symmetries. A daily example is the case of liquid-solid phase transition, in which liquid is macroscopically homogeneous and therefore can be described by continuous spacial groups; but crystalline solid has to be described by discrete spacial groups. Another important example is that the electroweak transition in the standard model, in which the $SU(2) \times U(1)$ gauge symmetry of the electroweak field is spontaneously broken into the $U(1)$ gauge symmetry of the electromagnetic field below the electroweak temperature.

In the modern classification scheme, phase transitions can be divided into two categories: *discontinuous phase transition* (or *fist-order phase transition*) and *continuous phase transition* (or *higher-order phase transition*). A transition is called fist-order when the first derivative of an appropriate thermodynamic state function, such as volume V and entropy S, is discontinuous. A transition is called nth-order when the (n-1)th derivatives are continuous, but the nth derivative is either discontinuous or infinite. Generally, a first-order phase transition is accompanied by a latent heat, therefore the transition between the two phases takes time. During the phase transition process, the two phases can co-exist as a mixture before the transition completes. In contrast, a second- or higher-order transition have no association with latent heat. Famous examples of second-order phase transitions are the superfluid and superconductor transition. Even higher-order phase transitions are very rare, and they are predicted in a few theoretical models, such as the 2-D XY model.

2.1.3 Density and order parameter

Density is probably one of few the material quantities known in early human history. Before 200 BC, when Archimedes of Syracuse shouted "*Εύρηκα* (Eureka)!", he realized how to measure the density of an irregularly-shaped wreath to find out whether King Hiero's goldsmith embezzled gold during the manufacture. In thermodynamics, density ρ comes into the equation of state as the reciprocal of the specific volume v, which is defined as the volume occupied by a unit mass

$$v = \frac{V}{m} = \rho^{-1} \tag{2.14}$$

then Equation (2.1) can be rewritten as

$$\rho = \rho(P, T) \tag{2.15}$$

which is the main equation of state measured by neutron scattering experiments and discussed in details in this chapter. On the other hand, the equation of state of entropy (2.2) is difficult to measure experimentally directly. With Equation (2.14) and (2.15), in principle, two response functions, the isothermal compressibility κ_T and the isobaric thermal expansion coefficient α, should be able to be easily obtained using Equations (2.3) and (2.4).

For gas-liquid-solid phase transitions, as a matter of fact, density ρ is the order parameter. Order parameter, just like its name implied, is a measure of the degree of order of a certain phase. Accordingly, the order parameter takes different values for different phases. Gas, liquid and solid have very distinct structures (symmetries). Different structures will normally result in different densities. So it is natural to consider density as the order parameter in the gas-liquid-solid phase transitions. The same logic may apply to the study of the liquid-liquid phase transition. Since different liquids have different structures, they must have different densities as well. Therefore, it's quite plausible to consider density as a candidate of the order parameter in the liquid-liquid phase transition. It should be mentioned that identifying an order parameter for a particular phase transition is a sort of art. For example, the superconducting order parameter is a complex field.

2.2 Confinement: hydrophilic and hydrophobic

The hypothetical liquid-liquid phase transition and liquid-liquid critical point of water are located in the "no man's land" at deeply supercooled temperatures, where bulk water does not exist in a liquid state. One of the methods to suppress the homogeneous nucleation process is to use confinement. The confinement material to inhibit the crystallization of water can be of a wide range of types, including 1-D, 2-D and 3-D, hydrophilic and hydrophobic, organic and inorganic[164, 53, 38, 166, 94, 41, 165, 93, 163, 92, 35, 42]. Thus, in the restricted geometry, the ice-like long-range

order cannot develop, which allows us to enter the "no man's land" to investigate the properties of water in a liquid phase at temperatures and pressures not accessible in the bulk. In this section, we will give a short introduction of the synthesis and characterization of two classes of nanoporous material made of silica and carbon respectively.

At this point, it should be mentioned that confinement may affect properties of water other than the suppression of homogeneous nucleation. So there might be a possibility that the phase behavior of confined water investigated may not represent the phase behavior of bulk water. Nevertheless, even if this turns out to be true, the research on confined water does not lose general interest. In fact, in many systems of biological and geological relevance, water is found confined in pores of nanoscopic dimension or in contact with hydrophilic or hydrophobic surfaces creating a layer[30, 31], one or two molecular sizes thick, of interfacial water, which can be supercooled far below the homogeneous nucleation temperature of bulk water.

On the other hand, a few recent studies suggest that water in hydrophilic confinement behaves quite similar to bulk water. A recent MD simulation of water confined in nanoporous silica material MCM-41-S with 15 Å pore diameter shows that besides the layer of water near the hydrophilic surface (2 Å to 3 Å thick), there is region in the center of the pores (10 Å to 11 Å in diameter), which is bulk-like[64]. Another MD simulation studies the structural variations for water confined between hydroxylated silica surfaces are contrasted with water confined between mica surfaces. They find that water confined between hydroxylated silica (the following MCM sample belongs to this class) behaves very much like bulk water[103].

2.2.1 Nanoporous silica material MCM

The ordered MCM-41-S powder sample is made of micellar templated nanoporous silica matrices, consist of grains of the order of micrometer size[160]. In each grain, parallel cylindrical pores are arranged in a 2-D hexagonal lattice with an inter-plane

distance $d = 30 \pm 2$ Å. The MCM-41-S is synthesized by reacting pre-formed β-zeolite seeds (composed by tetraethylammonium hydroxide (TEAOH, Acros), sodium hydroxide (NaOH) and fumed silica (Sigma)) with decyltrimethylammonium bromide solution (C_10TAB, Acros), then transferring the mixture into an autoclave at 120 °C for 2 days. After cooling down to room temperature, the mixture was adjust to $pH = 10$. Then the mixture was sealed into autoclave at 100 °C for 2 days. Solid sample is collected by filtration, washed by water, dried at 60 °C in air overnight, and then calcined at 540 °C for 8 hours. The molar ratios of the reactants are SiO_2 : NaOH : TEAOH : C_10TAB : $H_2O = 1 : 0.075 : 0.285 : 0.204 : 226.46$. The MCM-41-S is composed of amorphous porous silica, thus its surface is uniformly hydrophilic.

The pore diameter of the MCM-41-S sample can be tuned from 10 to 24 Å. Due to the Gibbs-Thomson effect, the freezing/melting point T_m is strongly depressed in the nanopores. The actual melting points of H_2O in MCM-41-S of different pore sizes are checked with differential scanning calorimetry (DSC), shown in Table (2.1). The melting points of D_2O in MCM-41-S are a few degrees higher than that of H_2O confined in the sample with same pore size.

	Pore Diameter (Å)	T_m (K)
MCM-41-SH	24	232
MCM-41-SH	22	225
MCM-41-SH	20	220
MCM-41-SH	19	220
MCM-41-SH	18	218
MCM-41-SH	16	<130
MCM-41-S	15	<130
MCM-41-S	14	<130
MCM-41-S	12	<130
MCM-41-S	10	<130

Table 2.1: H_2O melting points of porous material MCM-41-S

In most of our neutron scattering experiments, the major MCM-41-S sample used has the pore diameter of 15 ± 2 Å. Its pore volume is estimated to be 0.50 cm^3/g with

the Barret-Joyner-Halenda (BJH) analysis. Other MCM-41-S sample with different pore diameters are measured in cases to study the effect of the size of the confinement. The pore diameter can also be confirmed by fitting the neutron or X-ray diffraction profile with a cylindrical model of the pores. The sample is hydrated by exposing to water vapor in a closed container at room temperature until a full hydration level is achieved. The D_2O hydration level (mass of water/mass of dry sample) is 0.5, and the H_2O hydration level is around 0.33 measured by the thermogravimetric analysis (TGA) of the hydrated sample.

The MCM-41-S sample can be hydrophobically modified by treating the hydrophilic sample with chlorotrimethyl silane (CTS). The silanol-OH groups that cover the walls of the pore can be changed to methyl groups -O-Si$(CH_3)_3$. By varying the CTS/MCM ratio different levels of reaction can be achieved and therefore various degrees of hydrophobicity.

2.2.2 Nanoporous carbon material CMK

The nanoporous carbon CMK-1 was synthesized using MCM-48-S nanoporous silica as a template (cubic, Ia3d symmetry, consisting of two disconnected interwoven 3-D pore systems) and sucrose as carbon source (dehydrated by sulfuric acid dehydration). The powder sample of CMK-1 consists of grains of the order of micrometer size. Each grain has a 3-D interconnected bicontinuous pore structure. With the Barret-Joyner-Halenda (BJH) analysis, we obtain the pore volume and the average pore diameter to be 0.84 cm^3/g and 14 Å, respectively. The CMK-1 is composed of amorphous porous carbon, thus its surface is uniformly hydrophobic.

Similar to the hydration of MCM-41-S sample, the CMK-1 sample is also hydrated by exposing it to water vapor in a closed chamber until it reaches the full hydration level. The H_2O hydration level (mass of water/mass of dry sample) is 0.5 measured by thermogravimetric analysis (TGA) of hydrated sample. The hydration level is higher than that of the MCM-41-S sample, because carbon has a lower density than

silica.

X-ray diffraction (XRD) and transmission electron microscopy (TEM) are routinely performed to guarantee the sample quality. DSC check is routinely performed to make sure no freezing of bulk water occurs near 273 K. This proves that the amount of water outside the pores, if exists, is much less than water inside. Furthermore, no freezing of confined water occurs down to 130 K. This makes sure that water remains a liquid state in such deeply supercooled temperature. It is generally believed that near the wall of the porous material, there is a small layer of water with slightly different density[65], while in the center of the pores water distributes uniformly. H_2O, D_2O and their mixtures are chosen such that the sample has a considerably different coherent neutron scattering length density from that of the porous material, giving rise to a well-defined structure factor peak, which allows us to determine the density of water.

2.3 Density at ambient pressure

2.3.1 Small-angle neutron scattering technique

Small-angle neutron scattering (SANS) technique is used to measure the density of water confined in porous materials at ambient pressure[32]. A similar method has also been used to measure the density of confined toluene and benzene before[115, 2]. In this section, basic theories of SANS measurement of the density will be explained using the MCM-41-S powder system as an example. The model can be generalized to the density measurement in the CMK-1 confinement (Section 2.3.3) and with TAS technique (Section 2.4.1) with some modifications.

The diffraction pattern of the MCM-41-S powder sample consists of three parts: (a) the low-Q scattering of the fractal packing of the grains, which follows a power law Q-dependence; (b) a Bragg peak at around $2\pi/d$ coming from the 2-D hexagonal internal structure of the grains; and (c) the Q-independent incoherent background.

The contrast of the neutron coherent scattering length density (SLD) of heavy water against that of the silica matrix gives rise to a strong signal with a well-defined first Bragg diffraction peak arising from the (10) plane of a 2-D hexagonal lattice of water cylinders in the MCM-41-S silica matrix. The structure of the confining matrix is unaffected by temperature and pressure. In fact, one can immediately notice that the shape and the position of the Bragg peak do not change with temperature (Figure 2-4). The only temperature dependent variable is the amplitude of the Bragg peak (at 0.21 Å^{-1}), which is directly related to the water density.

In a small angle diffraction experiment, the neutron scattering intensity distribution $I(Q)$ is given by

$$I(Q) = nV_P^2(\Delta\rho_{sld})^2\bar{P}(Q)S(Q) \tag{2.16}$$

where n is the number of scattering units (water cylinders) per unit volume, V_p the volume of the scattering unit, $\Delta\rho_{sld} = \rho_{sld}^{D_2O} - \rho_{sld}^{MCM}$ the difference of scattering length density (SLD) between the scattering unit $\rho_{sld}^{D_2O}$ and the environment ρ_{sld}^{MCM}, $\bar{P}(Q)$ the normalized particle structure factor (sometimes called form factor) of the scattering unit, and $S(Q)$ the inter-cylinder structure factor of a 2-D hexagonal lattice. The SLD of the scattering unit $\rho_{sld}^{D_2O}$ is directly proportional to its mass density $\rho_m^{D_2O}$ as

$$\rho_{sld}^{D_2O} = \alpha\rho_m^{D_2O} \tag{2.17}$$

where[3]

$$\alpha = \frac{N_A\sum b_i}{M} \tag{2.18}$$

N_A is the Avogadros number, M the molecular weight of D_2O, b_i the coherent scattering length of the i-*th* atom in the scattering unit. The SLD of the silica material has been determined by a separate contrast matching experiment by hydrating the sample with different ratio of D_2O and H_2O. When the molar ratio is $[D_2O]$:$[H_2O]$=0.66:0.34,

[3]The coefficient α here should be distinguished from the isobaric thermal expansion coefficient in Section 2.1.1.

the Bragg peak is matched out. Since the structure of the confining matrix does not change with temperature in the investigated range, based on the above relations, we find that all the variables in the expression for $I(Q)$ are independent of temperature except $\rho_m^{D_2O}$. Hence we are able to determine the density of confined D_2O by measuring the temperature-dependent neutron scattering intensity $I(Q)$ at the Bragg peak.

The particle structure factor of a long ($QL > 2\pi$) cylinder is given by

$$\bar{P}(Q) = \frac{\pi}{QL}\left(\frac{2J_1(QR)}{QR}\right)^2 \tag{2.19}$$

where L and R represent the length and the radius of the cylinder respectively, and $J_1(x)$ is the first-order Bessel function of the first kind. The structure factor $S(Q)$ can be well approximated by a Lorentzian function. Therefore, the measured neutron scattering intensity is expressed as

$$I(Q) = nV_P^2\left(\alpha\rho_m^{D_2O} - \rho_s l d^{MCM}\right)^2 \frac{\pi}{QL}\left(\frac{2J_1(QR)}{QR}\right)^2 \left(\frac{\Gamma/2}{\left(Q-\frac{2\pi}{a}\right)^2 + (\Gamma/2)^2}\right) + B\cdot Q^{-\beta} + C \tag{2.20}$$

and at the Bragg peak Q_0

$$I(Q_0) = A\left(\alpha\rho_m^{D_2O} - \rho_s l d^{MCM}\right)^2 + B\cdot Q^{-\beta} + C \tag{2.21}$$

where Γ is the full-width at half-maximum (FWHM) of the Lorentzian function, C is the Q-independent incoherent background. The last unknown constant A is determined by normalizing the density of the highest temperature to that of the bulk water taken from NIST Scientific and Technical Database.

If the density distribution in the pores is not uniform, the correction of Equation (2.20) is estimated below. In the case of hydrated MCM-41-S, each scatter is a column of water confined in a cylindrical pore. If we assume the water molecules distribute non-uniformly only along the radial direction of the cylindrical pore as $\rho(r)$, the

normalized particle structure factor $\bar{P}(Q)$ can be written as

$$\bar{P}(Q) = \int_0^1 d\mu \left[\frac{1}{\pi R^2} \cdot \frac{\sin(Q\mu L/2)}{Q\mu L/2} \cdot 2\pi \int_0^R r \frac{\rho(r) - \rho}{\bar{\rho} - \rho_s} J_0(Qr\sqrt{1-\mu^2}) dr \right]^2 \quad (2.22)$$

where

$$\bar{\rho} = \frac{1}{V_p} \int_{V_p} \rho(r) dr^3 \quad (2.23)$$

is the average SLD of the water in the pore. ρ_s is the SLD of the environment. Since the sample is comprised of different crystallites oriented randomly, the scattering profile is obtained by averaging over all the possible orientation of the pores with respect to the incoming beam (integrated over $\mu = \cos\theta$).

As we can see from Equation (2.16), the effect related to a non-uniform distribution of water in the pore will be contained in the $\bar{P}(Q)$ term. We can demonstrate that, when using a realistic water distribution in the pore, this effect is an insignificant correction of the contrast factor $(\bar{\rho} - \rho_s)^2$ at the structure factor peak. Therefore, the change of the Bragg peak intensity mainly measures the contrast factor $(\bar{\rho} - \rho_s)^2$.

2.3.2 Density minimum in a hydrophilic confinement

More than 300 years ago, one density extreme of water, the density maximum at 277 K for H_2O (284 K for D_2O), was discovered. Only recently, we discovered the existence of the second density extreme of water, the density minimum at 210 K for D_2O (203 K for H_2O), by supercooling water in hydrophilic silica pores MCM-41-S. This discovery adds another anomaly to the more than 60 anomalies of water.

Below the density maximum temperature, the density of bulk liquid water decreases rapidly with temperature before the onset of homogeneous crystal nucleation that precludes further measurements. The density curve of ice Ih lies below that of the liquid, and almost certainly sets a lower bound on the density that the supercooled liquid could attain if nucleation were avoided, since ice Ih represents the limiting case of a perfectly ordered tetrahedral network of hydrogen bonds. Significantly, the

expansivity of ice Ih in this temperature range is positive, i.e. the density increases as temperature decreases. The low density amorphous (LDA) ice that forms from deeply supercooled liquid water at the (in this case extremely weak) glass transition, approaches very closely the structure of a random tetrahedral network (RTN), and exhibits a number of ice-like properties, including a "normal" (i.e. positive) expansivity. If the structure of the deeply supercooled water also approaches that of a RTN, it is therefore possible that a density minimum occurs in the supercooled liquid. Consistent with this possibility, a number of recent molecular dynamics (MD) computer simulation studies predict that a density minimum occurs in water (H_2O)[125]. In this section, the first experimental observation of a density minimum in supercooled water (D_2O) confined in the nanochannels of nanoporous silica is shown. The density minimum occurs at $T_{min} = 210 \pm 5$ K with a density value of 1.041 ± 0.003 g/cm^3 as shown in Figure (2-1).

Density minima in liquids are even more rare than density maxima. We are aware of reports of density minima in only a few liquid systems, such as Ge-Se mixtures. Confirming the existence of a density minimum in water would reveal much about the supercooled state of this important liquid. Its occurrence would signal the reversal of the anomalies that set in near the density maximum; i.e. that mildly supercooled water is anomalous, but that deeply supercooled water "goes normal"[7]. Observing a density minimum would also have significant implications for the possibility that a liquid-liquid phase transition (LLPT) occurs in supercooled water, along the same lines as was recently argued for vitreous silica.

This SANS experiment is performed at NG3, a 40-m SANS instrument, in the NIST Center for Neutron Research (NCNR). The incident monochromatic neutrons have an average wave length of $\lambda = 5$ Å with a fractional spread of $\Delta\lambda/\lambda = 10\%$. The sample to detector distance is fixed at 6 m, covering the range of magnitudes of neutron wave vector transfer (Q) from 0.008 Å^{-1} to 0.40 Å^{-1}.

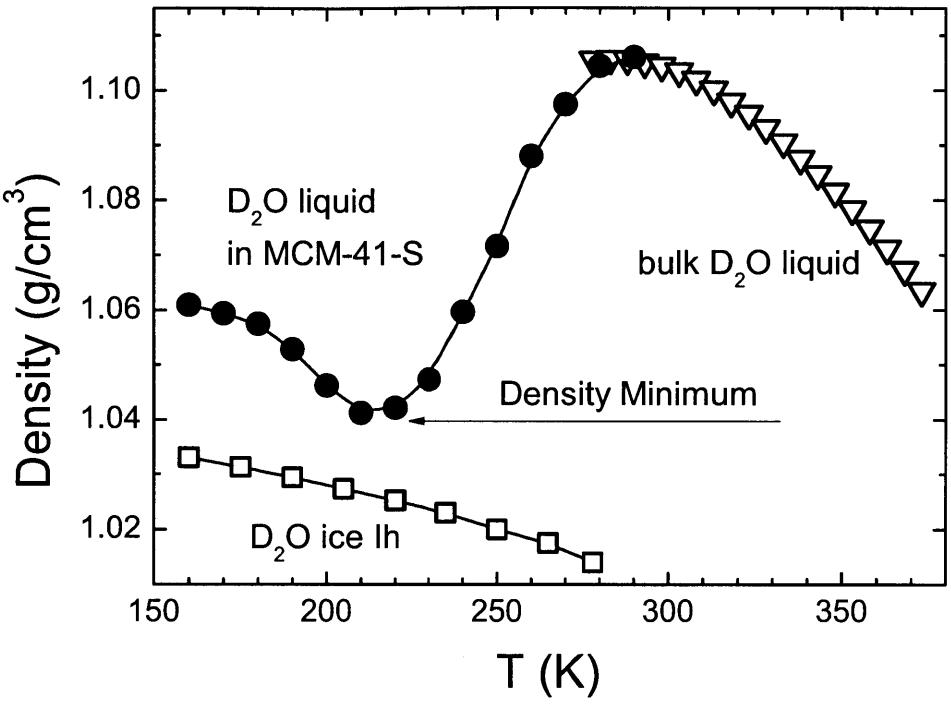

Figure 2-1: Comparison of density versus temperature curves at ambient pressure for bulk liquid D_2O (triangles), confined liquid D_2O (solid circles) and D2O ice Ih (squares). A density minimum of D_2O confined in MCM-41-S-15 is clearly observed at around 210 K.[93]

2.3.3 Absence of density minimum in a hydrophilic confinement

In section, a similar SANS method is used for the measurement of the density of H_2O confined in hydrophobic nanoporous material CMK-1 with about 14 Å pore diameter. We have measured the density of water in this hydrophobic confinement and find that the well-known density maximum of water is shifted to 260 K, and that the density minimum disappears. Moreover, when compared with the hydrophilic confinement MCM-41-S, the deduced thermal expansion coefficient shows a much broader peak spanning from 240 K to 180 K instead of a sharp peak at 230 K.

This experiment is performed using the General-Purpose SANS diffractometer CG-2 at High Flux Isotope Reactor (HFIR) in Oak Ridge National Laboratory (ORNL). Using neutrons with an incident wavelength of 4.75 Å, the effective observable single-setting wave vector transfer (Q) range is from 0.03 to 0.5 $Å^{-1}$, covering the structure factor peak of the CMK sample, whose amplitude is an indicator of the average density of the confined water. In terms of cold neutron flux on sample, this instrument is comparable to the best SANS instruments worldwide. To prevent leakage the samples are loaded in an airtight flat aluminum cell sealed with indium. The transmissions of the sample at each temperature are measured to monitor any possible sample change, and later on used in the subtraction of the empty cell scattering and instrument dark count. Data reduction is done in Igor using the standard procedures provided by the facility.

The CMK sample has a 3-D interconnected nanopores. So the product of the particle structure factor $\bar{P}(Q)$ and the structure factor $S(Q)$ in Equation (2.20) is is approximated by the average structure factor $\bar{S}(Q)$ within a grain

$$\bar{S}(Q) = \frac{2\ln 2}{\pi^{3/2}} \frac{w_L}{W_G^2} \int_{\infty}^{\infty} \frac{e^{-t^2}}{\left(\sqrt{\ln 2}\frac{w_L}{w_G}\right)^2 + \left(\sqrt{4\ln 2}\frac{Q-Q_c}{w_G} - t\right)^2} dt \tag{2.24}$$

the Voigt function representation of the diffraction profile. It is essentially a convolution of the Gaussian profile as a result of the Doppler broadening due to the thermal motions and a Lorentzian profile to account for the intrinsic broadening factors from the instrument and sample. The extracted density of confined H_2O in CMK-1 is shown in Figure 2-2.

The first novel phenomenon observed in the hydrophobic confinement is that the temperature of the density maximum is lowered 17 K from 277 K to 260 K. This is in contrast to what is known to occur with hydrophilic confinement in MCM-41-S, where the temperature of the density maximum is the same as that of bulk water, for both H_2O at 277 K and D_2O at 284 K, als shown in Figure 2-2. A plausible reason for this

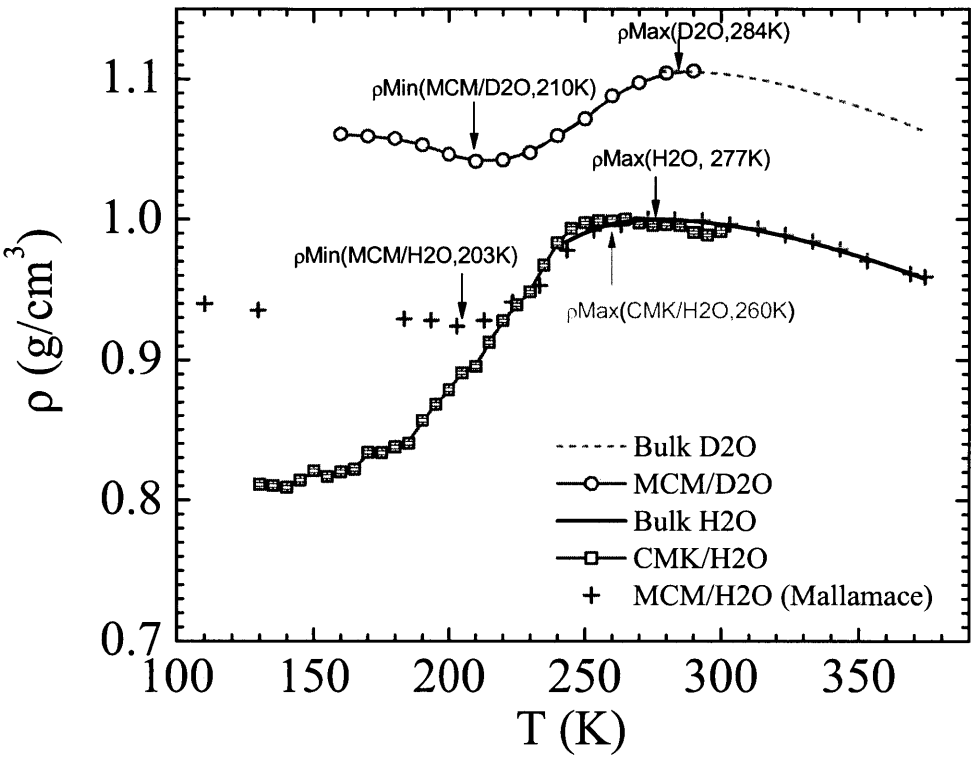

Figure 2-2: Comparisons of densities of different isotopic species of water in different confinements. The red squares show the density of H_2O confined in CMK-1. These data show that the density maximum of water in hydrophobic confinement still exists, but is shifted to a lower temperature at 260 K, while the density minimum is absent.[166]

shift is that the formation of the open tetrahedral hydrogen bond network is delayed to a lower temperature in the hydrophobic confinement. This fact is independent of the scaling method we used in determining the absolute density.

The second and probably more interesting phenomenon is that the density minimum previously observed in hydrophilic confinement both for H_2O at 203 K) and for D_2O at 210 K is not observed in the hydrophobic confinement. This result implies that the random tetrahedral network of hydrogen bonds is not fully developed

at temperatures above 130 K or possibly lower in hydrophobic confinement. The interaction between the carbon surface and water is relatively unfavorable, thus the tetrahedral hydrogen bonding pattern is disrupted close to the hydrophobic surface. Without the compensatory interactions that might operate at the hydrophilic surfaces, the formation of hydrogen bonds is more difficult and will hardly saturate. In the extreme case, there might exist a lower density layer near the surface, which is usually called drying or dewetting. The water depletion layer at room temperatures was confirmed by experiments in the vicinities of different hydrophobic surfaces and by simulations of water in carbon nanotubes. This depletion layer will result in lower average densities of water at deeply supercooled temperatures.

In addition, the density profile in hydrophobic confinement as a function of temperature is very different from that in hydrophilic confinement. This is emphasized by the deduced thermal expansion coefficient which is independent of the scaling factor used in determining the absolute density (shown in Figure 2-3). In the hydrophilic confinement MCM-41-S, the expansion coefficient α shows a sharp peak at $T_L = 230$ K which is interpreted as crossing of the Widom line[57, 158]. In this experiment, in hydrophobic confinement CMK-1, the expansion coefficient α shows a very broad peak spanning from about 240 K to 180 K. Whether the broad peak is due to the hydrophobic-hydrophilic transition awaits for future research. One should also note that in this plot the points at which α across zero represent the density extremes. Again, we observe the temperature of the density maximum is shifted lower by 17 K while the density minimum is absent in CMK/H_2O.

In summary, using SANS technique, we measured the density of water confined in both hydrophilic and hydrophobic nano pores. The density data may provide clues to controlling the thermodynamic properties of water using nano-confinement with different degrees of hydrophobicity. Moreover, the anomalous density behavior of deeply supercooled confined water are important to find out a unified explanation of the puzzling phase behavior of water. The density measurement at ambient pressure

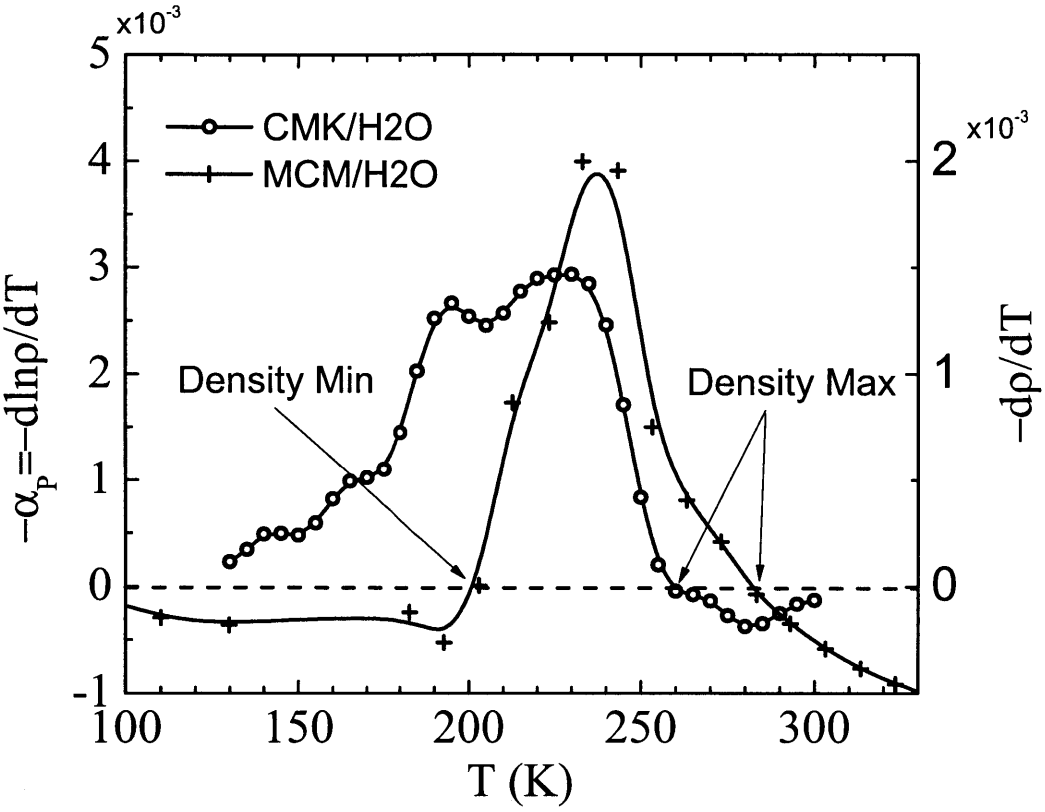

Figure 2-3: The thermal expansion coefficient of CMK/H2O compared with the $d\rho/dT$ of MCM/H_2O. The CMK/H_2O density is smoothed using a 2-point FFT filter in order to eliminate some statistical errors. The peak of CMK/H_2O is much broader than MCM/H_2O.[166]

also motives us to perform the density measurements at elevated pressures.

2.4 Density at elevated pressures

A reliable measurement of the density is extremely useful to determine the phase behavior of water, as demonstrated in the previous section. However, when applying the SANS technique to the density measurement at high pressures, new challenges emerge[61]. First, the measurement requires a high-pressure cell, obviously. A pres-

sure cell for a SANS experiment at low temperature is not trivial. Normally, a pressure cell is made of very thick wall to hold the pressure. However, on a SANS instrument, such a standard pressure cell would be so thick that not enough neutrons could penetrate through. This self-shielding effect prevents us to obtain data with satisfying signal-to-noise ratio. Alternatively, if we open the wall of the pressure cell and use sapphire windows, it would be not easy to prevent the leakage at low temperatures, because every part of the cell should have the correct expansivity in order not to create chinks during temperature change. Second, from the previous SANS analysis, one can see that in order to determine the density of water, only the height of the structure factor peak is required. Therefore, in principle, the measurement of the neutron scattering intensity at the single Q_{max} would be sufficient.

Keeping those in mind, in order to measure the density of water at high pressures and low temperatures, a much more efficient method for the density determination is developed employing a cold neutron triple-axis spectrometer (TAS). Using this improved method, we measured the density as a function of closely spaced temperatures (as accurate as every 1 K) from 300 K to 130 K in a range of pressures from ambient to 2900 bar. In this way, we explore the equation of state of heavy water $\rho(P,T)$ confined in MCM-41-S in the region of the P-T phase space where the source of the anomalous properties of water may be found.

2.4.1 Triple-axis spectroscopy

A triple-axis spectrometer can probably be considered to be the mother of most neutron scattering spectrometers. The triple-axis stands for the monochromator axis, the sample axis, and the analyzer axis. Taking advantage of the setup of the instrument, it is possible to perform scans of both the momentum transfer Q and the energy transfer E. Therefore, it is widely used as an inelastic neutron scattering instrument for studies of dynamics.

Considering our purpose of measuring the density of water, we only need to op-

erate the TAS in an elastic mode. The neutron scattering experiment is carried out at the NIST Center for Neutron Research (NCNR) using the cold neutron spin polarized triple-axis spectrometer (SPINS) with incident neutron energy of 3.7 meV. A feasibility test experiment is performed on a thermal neutron triple-axis spectrometer (BT7/BT9) at NCNR. The hydrated MCM-41-S sample is loaded in the NCNR pressure cell HW-02 with a sample volume of 1.5 cm^3. Pressure was applied with helium gas. The sample temperature was controlled using a top loading closed cycle refrigerator. A small amount of helium was used to insure thermal exchange between the sample and the wall of the refrigerator, whose temperature was controlled with accuracy better than 0.01 K. The density data are reported as function of the sample temperature, which is recorded by a sensor located just above the pressure cell.

By fitting the neutron diffraction intensity with Equation (2.20) at the highest and lowest temperature at each pressure, the parameters B, β and C are obtained. We are thus able to subtract the "background" with confidence. We determine the last unknown parameter A by normalizing the density of the highest temperature at each pressure to that of the bulk D_2O taken from NIST Scientific and Technical Database. When the density of supercooled D_2O is not available, the density was normalized to the density of H_2O (at the same temperature and pressure) times 1.109.

Once the data are corrected for the temperature independent background arising from the fractal packing of the MCM-41-S crystallites and the incoherent scattering, the only temperature-dependent quantity is the height of the Bragg peak, which is proportional to the square of the difference of SLD between the heavy water and the silica matrix, and therefore a sensitive indicator of the average mass density of the confined water. We can therefore sit at the Bragg peak position and monitor the peak intensity as a function of temperature, rather than performing a scan in Q at each temperature. While our measurements are highly precise and sensitive with regard to relative changes, there is an overall uncertainty that we estimate to be 0.02 g/cm^3 (standard deviation) in the overall density scale, arising from uncertainties in the

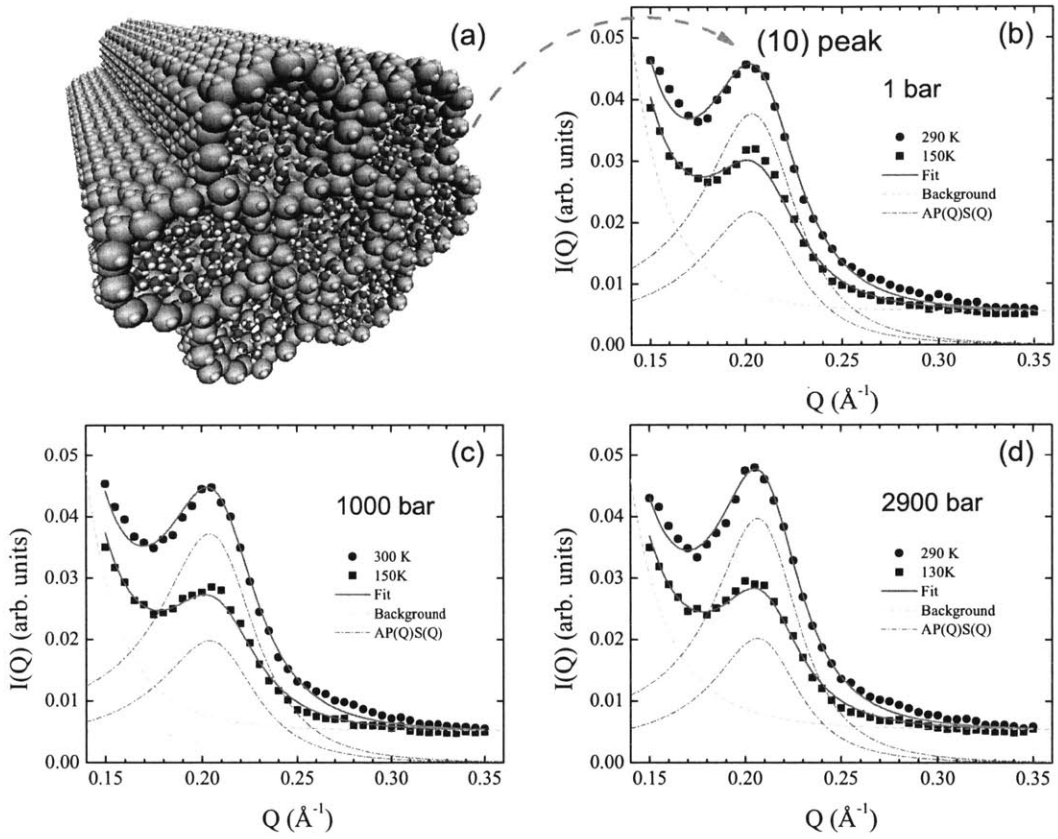

Figure 2-4: (a) Schematic representation of a heavy water hydrated MCM-41-S nanoporous silica crystallite (pore diameter $2R \approx 15 \pm 2$ Å). (b-d) The elastic neutron diffraction intensity $I(Q)$ at three pressures: 1 bar, 1000 bar, and 2900 bar. The structure factor peak at around 0.21 Å^{-1} comes from the (10) plane of the 2-D hexagonal arrangement of the water cylinders in the crystallite. The peak height is proportional to the square of the difference of neutron scattering length density (SLD) between the confined heavy water and the silica matrix, and therefore is a sensitive indicator of the average mass density of water in the pores. By fitting with Equation (2.20), the temperature-independent background (green dashed line) and the temperature-dependent "clean" elastic diffraction intensities (blue dash-dotted line) can be separated accordingly.

scattering length density of the silica matrix, and the model we have used to analyze the data. It should be pointed out, though, that the uncertainty can be considered as a scaling factor and a shift, and that the relative shape of the density curves is

almost directly related to the measured scattering intensity.

2.4.2 High pressure: "hysteresis"

It is hypothesized, by all the three scenarios of water (SF, LLCP and CPF), that in the supercooled temperature range bulk water is composed of a mixture of two structurally distinct liquids: the low-density liquid (LDL) and the high-density liquid (HDL). They are respectively the thermodynamic continuation of the low-density amorphous ice (LDA) and high-density amorphous ice (HDA) into the liquid state[157, 117, 99, 56, 154]. Historically, a first-order phase transition between LDA and HDA was first suggested by Mishima and later confirmed with a variety of measurements[108, 107, 114, 111, 110]. Subsequently, Mishima and Stanleys experiment on the decompression-induced melting curves of several high-pressure phases of ice supports the coexistence of two different phases of supercooled liquid water[112, 113]. Recently, the observation of two structural motifs of liquid water was observed by X-ray emission spectroscopy[78, 152] and small-angle X-ray scattering. The existence of the LDL was also observed by FTIR absorption measurements[14]. More recently there are a number of other experimental evidences suggesting that there is a 1st-order liquid-liquid phase transition between HDL and LDL in solvent water of protein crystals[84] and in bulk water-ice mixture[14]. However, despite intensive research, a direct evidence of first-order liquid-liquid phase separation has not been observed so far[69, 124].

In order to study the possible first-order LDL-HDL phase transition, warming and cooling cycles are performed at a series of pressures. For each pressure, the sample is free cooled from 300 K to 130 K at ambient pressure, and then pressurized to the desired pressure. We then waited about 2 hours for system equilibration. The warming scan with 0.2 K/min is first performed from 130 K to 300 K. When the warming scan is finished, we waited another 2 hours at room temperature for system equilibration. After that, the cooling scan with 0.2 K/min is performed from 300 K to 130 K. When the full cycle is done, the sample is brought to ambient temperature

and pressure before measuring another pressure.

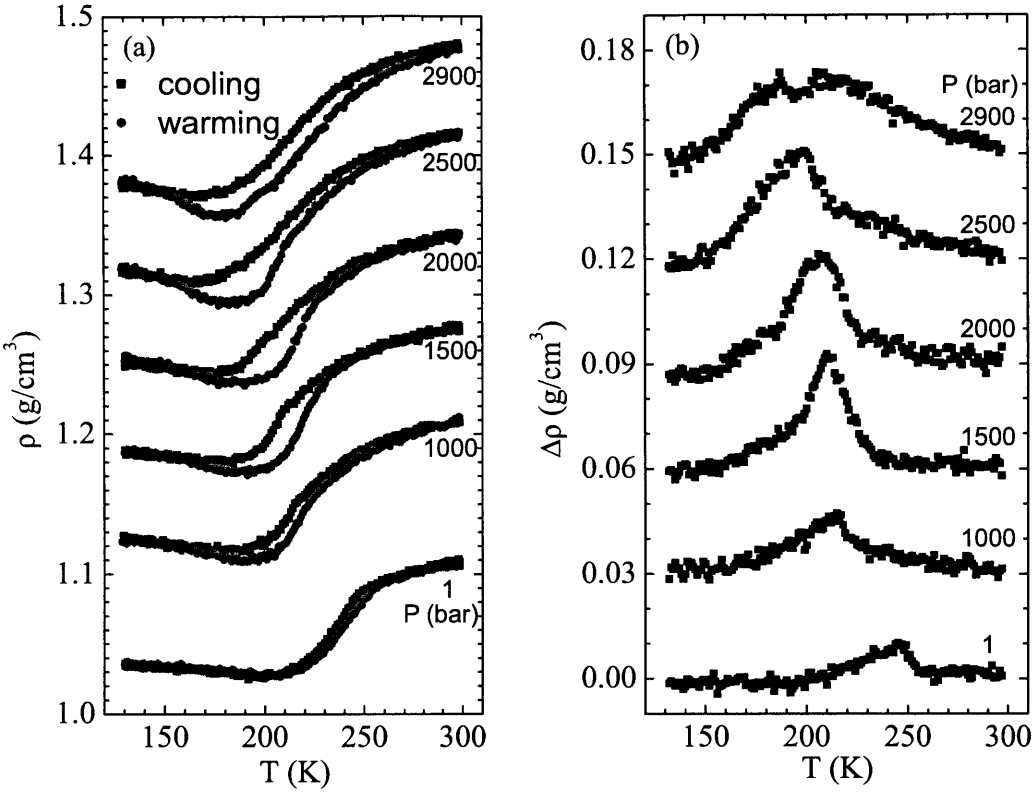

Figure 2-5: Measured isobaric density profiles of confined heavy water by both warming and cooling scans.The corresponding density difference between the two scans. The data are shifted by 0.05 and 0.03 g/cm^3 between adjacent pressures for clarity in panel (a) and (b) respectively. A hysteresis phenomenon becomes prominent at $\approx$ 1500 bar and above, which is a direct evidence of the phase separation when a first-order phase transition line is crossed.

The measured density profiles with both cooling and warming scans at a series of pressures are shown in Figure 2-5(a). The difference between the two scans are shown in Figure 2-5(b). Up to 1000 bar, the hysteresis between the cooling and warming scans is small, which could be attributed to the temperature lag for the system to equilibrate when ramping the temperature continuously. This intrinsic hysteresis should be small and relatively independent of pressure. However, the hysteresis be-

comes significantly larger at and above 1500 bar. The large hysteresis is likely because of the rather long time required for the phase separation to occur in confinement, and therefore it is an indication of a first-order phase transition.

The observed hysteresis phenomena are not artifact due to the solvation of helium gas. Among all the common gases used for high-pressure experiments, helium has the lowest solubility. Table 2.2 reports the solubility of different gases at 0°C, 1 atm. Using Henry's law, at 3000 bar, the solubility of helium is $0.0755 \times 10^{-4} \times 3000 = 0.0227$ mole fraction. With such a low solubility, its effect on the density of water is negligible.

	He	N_2	Ar	
Solubility (mole fraction)	0.07553	0.1914	0.4309	$\times 10^{-4}$

Table 2.2: Solubility of common gases for high pressure experiment in H_2O

2.4.3 Low pressure: "kink"

Measurements at more pressures are performed by cooling scans at pressures from ambient to 2900 bar. The measured density data are shown in Figure 2-6(a). The isobaric density profiles show a steep decrease as the water is increasingly supercooled, reaching a clear minimum for each pressure. The minimum temperature T_{min} decreases from 210 K to 170 K as the pressure is increased from ambient to 2900 bar. The density minimum is an indication of the full development of the defect-free random tetrahedral network (RTN) of the hydrogen bonds. Below T_{min} the perfect RTN begins to contract as the temperature is further lowered. Our results therefore imply that at higher pressures, the RTN can only be reached at lower temperatures. This is a consequence of the fact that the enthalpically favourable hydrogen bonded RTN has a lower density compared to its less developed counterpart[104].

Another remarkable feature of this plot is that the isobaric density profile shows a sudden change of slope ("kink") at a certain temperature at and below $\approx$ 1600

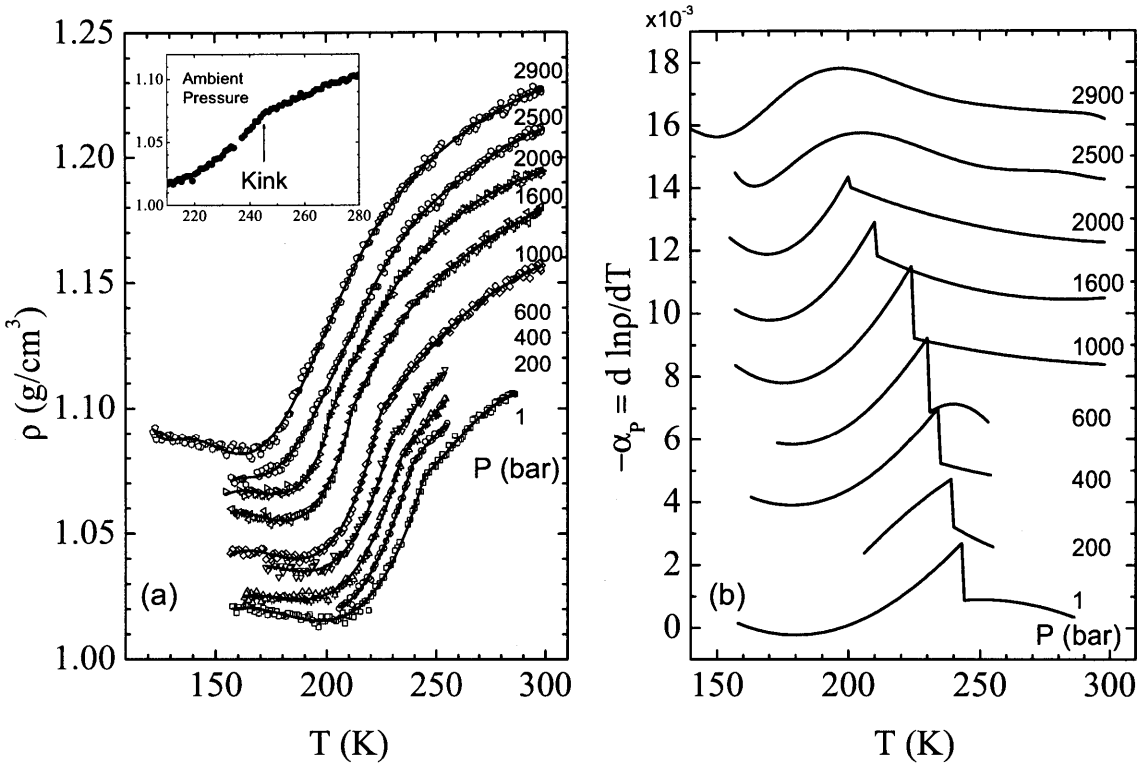

Figure 2-6: (a) Measured isobaric density profiles of confined heavy water by cooling scans. A well-defined "kink" in the density profile can be observed from ambient pressure to $\approx$ 1600 bar. The solid lines are fittings of the densities. The inset zooms in the region of the "kink" at ambient pressure. Error bars in the density, due to counting statistics, are smaller than the point size. A larger uncertainty in the density scale is discussed in the text. (b) The isobaric thermal expansion coefficient evaluated from the fitted density curves. The data are shifted by 0.002 between adjacent pressures for clarity. The sudden jump (discontinuity) in α is clearly observed below $\approx$ 1600 bar, but is absent above 2000 bar.

bar. In order to understand this phenomenon, we fitted the density profiles with 2-piecewise third-order polynomial at pressures from ambient to 2000 bar. The isobaric thermal expansion coefficients α are then evaluated analytically from the fitted polynomials, shown in Figure 2-6(b). A discontinuity in α directly coming from the "kink" is presented at and below $\approx$ 1600 bar. The discontinuity in the response

functions literally defines a second-order phase transition. Whether the transition belongs to the λ-transition universality class requires more accurate studies of the critical exponents. The most prominent example of a second-order phase transition is the superfluid transition of helium-4, which shows an analogous kink in the density profile and a discontinuity in α and c_P[81, 6, 60]. The possible existence of a λ-transition in supercooled water was argued previously in the literature based on specific heat measurements. However, due to finite temperature increment, the discontinuity in c_P has never been observed, instead, it is smeared out into a peak. Note that the growth of the correlation length ξ (the peak height of α) on approaching 1600 bar from ambient pressure is slightly observable, probably because the growth of the correlation length ξ is limited in the confined geometry.

Above $\approx$ 1600 bar, the "kink" in the density profile is no longer observable. Accordingly, the discontinuity in α also disappears, implying some sort of critical point. Note that, at 2000 bar, the discontinuity in α becomes minimal, independent of the enforced fitting with the piecewise polynomial. Therefore, at 2500 and 2900 bar, the density profiles are fitted with single polynomials (9th-order) in order to take derivatives.

Finally, Figure 2-7 summarizes the lines of density kinks and maximum density hysteresis in the $P-T$ and $\rho-T$ planes. Our density measurements clearly show a change of behavior at $T_c = 210 \pm 10$ K, $P_c = 1500 \pm 500$ bar. Above P_c, the hysteresis phenomenon is a strong evidence of the existence of the first-order phase transition, which is predicted by the LLCP scenario. Below P_c, the discontinuity of the expansion coefficient suggests a second-order phase transition[81, 6, 60]. Therefore, it is plausible that the hypothesized liquid-liquid critical point of water[109] is actually a "tricritical point". Well-known examples of tricritical points include, but are not limited to, the mixture of ^{3}He and ^{4}He[118, 91, 85, 72, 44, 83], and metamagnet $FeCl_2$[22]. However, it does not rule out the possibility that the apparent discontinuity of the expansion coefficient is related to the crossing of the Widom line[76, 147].

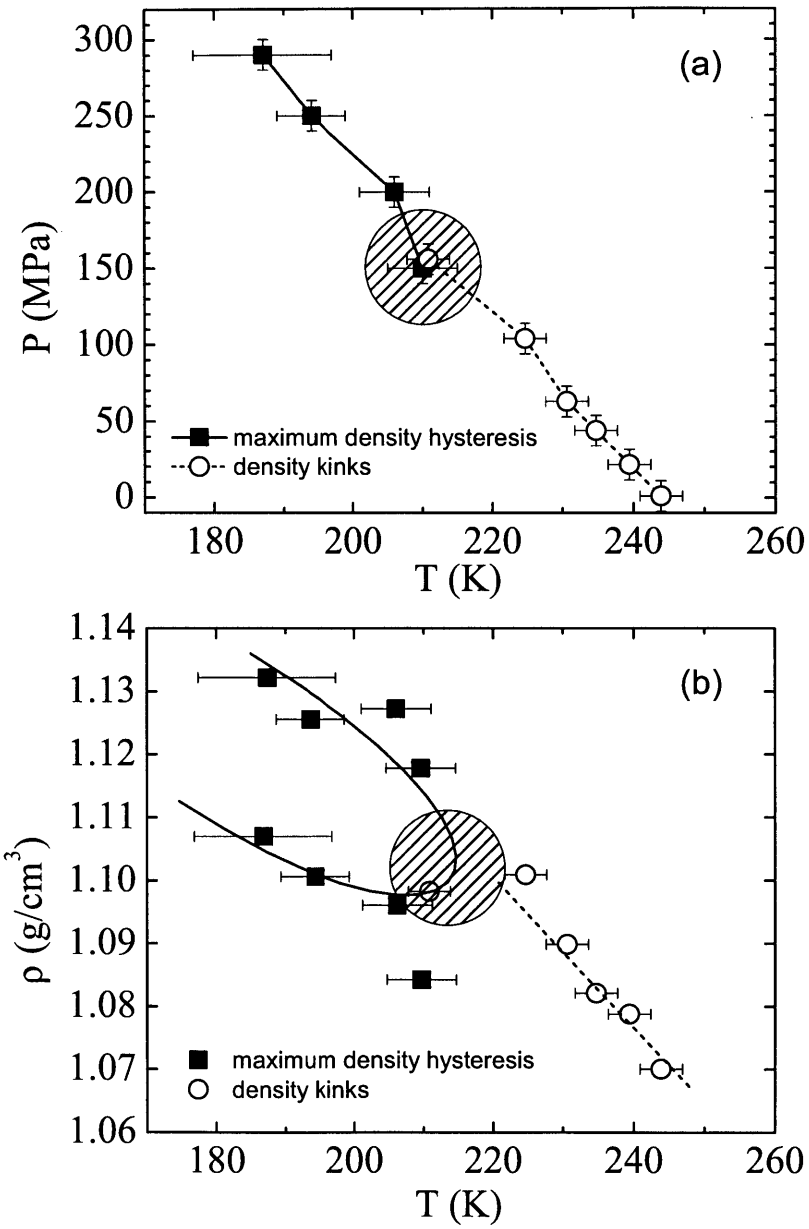

Figure 2-7: Phase diagrams of the confined heavy water. The empty circles, connected by the dotted line, are determined from the position of the kinks in the density profiles. The filled squares, connected by the solid line, are determined from the position of the maximum density hysteresis. Therefore, the shadow area connecting the two lines is where one may find a critical point of some kind.

In summary, by using a triple-axis spectrometer, we were able to obtain sensitive and precise measurements of the density of confined heavy water, achieving a remarkably good signal-to-noise ratio. The findings may lead to a unified framework for understanding the properties of confined water. The density data are the main results and will be useful for a better modeling of the properties of water in various biological and geological conditions: (a) in rocks and clays, relevant for mining purposes and environmental questions; (b) on the surface of proteins and membranes, relevant to address at molecular level a number of biological processes; (c) in different artificial porous environments used for catalytic purposes.

THIS PAGE INTENTIONALLY LEFT BLANK

Chapter 3

Pre-glass-transition phenomena: dynamics

The deepest and most interesting unsolved problem in solid state theory is probably the theory of the nature of glass and the glass transition. This could be the next breakthrough in the coming decade. The solution of the problem of spin glass in the late 1970s had broad implications in unexpected fields like neural networks, computer algorithms, evolution, and computational complexity. The solution of the more important and puzzling glass problem may also have a substantial intellectual spin-off. Whether it will help make better glass is questionable.

— Philip W Anderson[156]

3.1 Representative Cases

Parallel to the density measurements discussed in Chapter 3, the dynamics of water in confined geometry is also investigated using a variety of quasi-elastic and inelastic neutron scattering spectrometers. Two representative cases are used for the dynamic studies: (1) the interfacial water on protein surfaces – a 2-D confined water[164,

37]; (2) the water in the interconnected pores of an aged cement paste – a 3-D confined water[163, 165]. Both of the two cases are good examples to demonstrate how water affects its surroundings. In fact, protein is the building block of lives, while cement is the building blocks of our cities. Interesting enough, both of them are greatly influenced by the fluctuations of water. Using these two examples, we found that the dynamic anomalies of water are intimately correlated to the thermodynamic anomalies of water.

3.1.1 Protein hydration water

The importance of the role played by hydration water in protein folding behavior was realized after introduction in the literature of "hydrophobicity", a concept related to protein stability for the first time by Kauzmann[82]. From that moment on, a protein should have been defined as the system "peptide + water"[58] since the simple biomolecule is not able to perform its biological activity without at least one layer of water surrounding it. In particular the conformational flexibility of a protein (and therefore its biological functionality) is extremely sensitive to the characteristics of its hydrogen bonds with hydration water. This latter experimental fact is understandable considering that proteins evolved from their very beginning in an aqueous environment.

Without water, dry protein cannot function, but a single layer of water surrounding it brings life to the protein and restores its biological activity. It has been shown that the enzymatic activity of proteins depends crucially on the presence of at least a minimum amount of solvent water[149]. It is believed that 0.3 gram of water per gram of protein is sufficient to cover most of the protein surface with one single layer of water molecules and to fully activate the protein functionality. Therefore, the knowledge of the structure and dynamics of water molecules in the so-called hydration layer surrounding proteins is therefore of utmost relevance to the understanding of the protein functionality.

Using quasi-elastic neutron scattering technique, we extensively studied they relaxational dynamics of protein hydration water. Hen egg white lysozyme used in this experiment is obtained from Fluka (L7651; three times crystallized, dialyzed, and lyophilized) and used without further purification. The sample is lyophilized overnight to remove any water left (about 7%). The dried protein powder then was hydrated isopiestically at 5 °C by exposing it to water vapor in a closed chamber until hydration level $h = 0.35 \pm 0.01$ is reached (i.e., 0.35 gram of water per gram of dry lysozyme). Two kinds of lysozyme sample were prepared in this way, one using H_2O and the other using D_2O. The hydration level was determined by thermogravimetric analysis and also confirmed by directly measuring the weight of absorbed water. This hydration level was chosen to have about one monolayer coverage on the protein surfaces.

3.1.2 Cement hydration water

Ordinary Portland cement powder consists of calcium silicates, aluminates and alumino-ferrites. White cement, in contrast to ordinary Portland cement, is lack of calcium alumino-ferrite phases. When it is combined with water, it forms a plastic paste that sets and eventually hardens to a rock-like consistency. During this curing process a series of chemical hydration reactions take place to form the corresponding hydrated phases, mainly calcium silicate hydrate (C-S-H), and to develop a 3-D interconnected solid random network. Thus, water plays the central role during the overall hydration process, when cement gains the desired hardness and strength. Understanding the dynamic behavior of water confined in the cement paste is therefore crucial to achieve a complete control over its mechanical properties[128].

An example of the 3-D confinement of water in cement paste can be pictured through the Jennings Colloidal Model (JCM)[80, 151]. As displayed in the inset of Figure 3-1, C-S-H is composed of colloidal particles with radius of 1.5 nm that aggregate to form globules (small spheres in Figure 3-1(a)). These globules cluster to form

low-density (LD) C-S-H regions within 24 hours. The size of these pores inside the LD C-S-H is estimated to be around 1 nm[140], which corresponds to the interplanar space between the growing C-S-H lamellae. Because of the hydration process the LD C-S-H domains assemble to give a structure with larger pores connected by narrow channels called inter-LD regions. The size of these pores are reported to vary in a large range (approximately between 1 and 10 nm). The LD C-S-H aggregates grow with time, and after 1 month all the water in the inter-LD C-S-H is consumed by the hydration reaction.

The JCM is consistent with the Differential Scanning Calorimetry (DSC) thermogram recorded after 11 days from the preparation (Figure 3-1(a)). Two main features (peaks) are present, at 247 K and 231 K, among which the second peak represents the main contribution. No peak is detected above 253 K, in the temperature range typical for the freezing of bulk water. Thus, at this hydration time all the unreacted water in the sample is strictly kind of confined water in the solid matrix. According to the JCM, the two peaks visible in the cooling part of the thermograms are due to "water reservoirs", i.e. relatively large pores interconnected through small channels, with nanometric diameter. In particular, the peak in the region between 253 and 238 K is due to water that is only accessible via the inter-LD pores. The time evolution of this kind of water is strongly connected to the w/c ratio and in our conditions is totally consumed after 28 days. On the other hand, the peak at 231 K corresponds to pores inside the LD C-S-H domains.

Near Infrared (NIR) experiments confirm that after 8 days of setting the water in the cement paste is confined. Figure 3-1(b) reports the NIR spectrum registered on a 3 hours-cured sample, at 123 K. The absorption at 6070 cm^{-1} is considered as a fingerprint of hexagonal ice. The absence of the 6070 cm^{-1} peak after 8 days indicates that, at this hydration time, water is totally 3-D confined in the LD C-S-H domains and cannot crystallize anymore. This is the kind of water we observed in the neutron scattering experiment. A detailed description of the time evolution of both

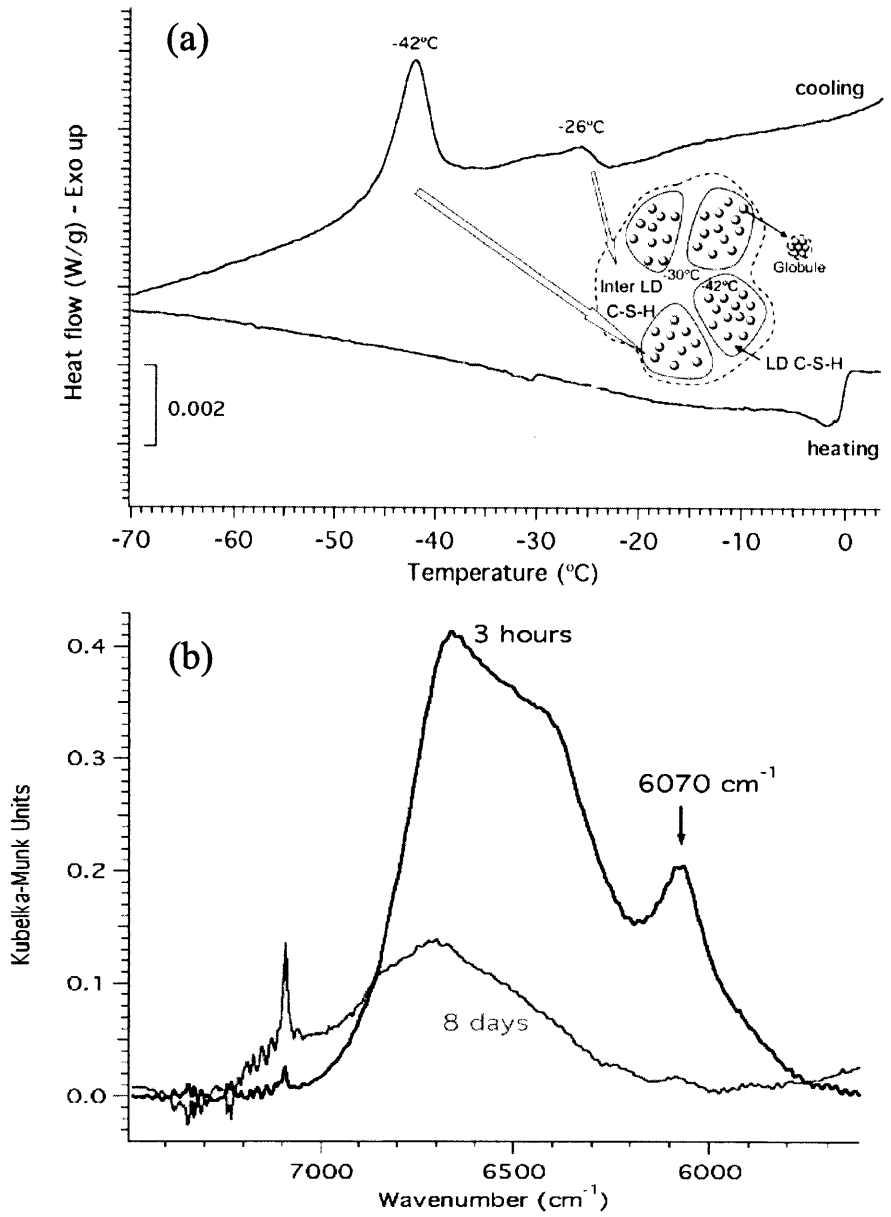

Figure 3-1: (a): DSC thermogram (cooling scan) of cement paste cured for 11 days. The inset displays a schematic representation of the Jennings Colloidal Model. According to the JCM, the peak at 247 K is due to inter-LD pores water and the peak at 231 K to LD pores water. (b): NIR spectra acquired at 123 K on cement paste cured for 3 hours (black curve) and 8 days (grey curve).[165]

low temperature NIR and DSC experiments performed on the same cement/water paste can be found elsewhere.

3.2 Slow dynamics

3.2.1 Quasi-elastic neutron scattering

Quasi-elastic neutron scattering (QENS) measures the broadening of the elastic line, which represents the diffusional motion of the particles. The high-resolution backscattering spectrometer BASIS at Spallation Neutron Source (SNS) in Oak Ridge National Laboratory (ORNL) is used to measure the broadening of the elastic peak of the hydrogen atom dynamic structure factor $S_H(Q, E)$. Using incident neutrons of 2.08 meV, BASIS is capable of measuring a dynamic range as large as $\pm$ 150 μeV with an elastic energy resolution of 3 μeV (FWHM). Another backscattering spectrometer HFBS at NIST Center for Neutron Research is aslo often used. Its best energy resolution is 0.8 μeV, but with a energy dynamic range of $\pm$ 11 μeV. Therefore, these two spectrometers cover slightly different time windows.

3.2.2 4-point correlation function and dynamic response functions

A family of dynamic response functions are defined in parallel to the thermodynamic response functions discussed in Section 2.1.1. The so-called dynamic response function $\chi_T(Q, t)$, or sometimes called dynamic susceptibility, is defined in analogy with the thermodynamic response functions such as the specific heat and thermal expansion coefficient, which are temperature derivative of the thermodynamic state functions, such as the entropy S or specific volume v. In order to describe the dynamic response of a system to an external perturbation ΔT, we can take the derivatives of the time-dependent state functions, such as the single-particle density correlation function

$F_H(Q,t)$. $\chi_T(Q,t)$ is one of this family of dynamic response functions and it is defined as the derivative of $F_H(Q,t)$ with respect to the temperature T at constant pressure, namely,

$$\chi_T(Q,t) = -\left(\frac{\partial F_s(Q,t)}{\partial T}\right)_P \tag{3.1}$$

$\chi_T(Q,t)$ is the linear response of a system to a small perturbation field, in this case the temperature change ΔT. $\chi_T(Q,t)$ also shows a peak at around $\tau_(Q,T)$ when plotted as a function of time at constant Q, and the height of which is proportional to some sort of dynamic correlation length. Experimentally, $\chi_T(Q,t)$ is a much easier quantity to measure with QENS.

3.2.3 Dynamic heterogeneity and dynamic crossover

Recently, a lot of efforts have been devoted to studies of the spatially heterogeneous dynamics[122, 17], i.e. the so-called dynamic heterogeneity, when approaching the glassy state. Dynamic heterogeneity refers to spatially-separated particles moving cooperatively. The idea that dynamic heterogeneity might play an important role near the glass transition can be traced back to Adam and Gibbs[1]. They provided a theoretical argument of the existence of cooperatively rearranging regions in glassy liquids.

A genuine multipoint correlator, the four-point dynamic correlation function $\chi_4(Q,t)$, was commonly used to quantify the dynamic heterogeneity

$$\chi_4(Q,t) = N\left\langle \left(\delta\hat{F}_H(Q,t)\right)^2 \right\rangle \tag{3.2}$$

where N is the total number of particles, $\delta A(t)$ stands for the fluctuation $\delta A(t) = A(t) - \langle A\rangle$. We first introduce a time correlation function:

$$\hat{F}_H(Q,t) = \frac{1}{N}\sum_l \exp(-i\mathbf{Q}\cdot\mathbf{r}_l(t))\exp(i\mathbf{Q}\cdot\mathbf{r}_l(0)) \tag{3.3}$$

which is an unaveraged hydrogen atom single-particle density correlator. Therefore the ordinary hydrogen atom single-particle intermediate scattering function (ISF) can be calculated as an ensemble average of it, i.e.

$$F_H(Q,t) = \langle \hat{F}_H(Q,t) \rangle \tag{3.4}$$

By definition, $\chi_4(Q,t)$ quantifies the expectation of the square of the fluctuations of the single-particle density correlator. If we do not take the square in Equation 3.2, the ensemble average of it would go to zero in the long time limit. The general feature of $\chi_4(Q,t)$ as a function of time displays a peak, the position of which indicates the characteristic structural relaxation time $\tau(Q,T)$ of the system, and the height of which is related to the volume where correlated particle motions (the dynamic heterogeneity) take place. Despite of the usefulness of $\chi_4(Q,t)$ in characterizing the dynamic heterogeneity, the direct measurement of it by a neutron scattering experiment is still a challenge. However, we can estimate $\chi_4(Q,t)$ from a related quantity $\chi_T(Q,t)$ which is experimentally accessible by QENS. The two functions are related to each other by the fluctuation-dissipation theorem, since $\chi_4(Q,t)$ measures the spontaneous fluctuations and $\chi_T(Q,t)$ measures the temperature-induced fluctuations[20, 21, 19, 153].

In our experiments, the total number of particles N, the pressure P and temperature T are kept as constants, therefore one can apply the fluctuation-dissipation theorem in the NPT ensemble to relate the induced fluctuations to the spontaneous fluctuations:

$$\chi_T(Q,t) = \frac{N}{k_B T^2} \left\langle \delta\hat{F}(Q,t)\delta H(0) \right\rangle \tag{3.5}$$

where $H(t)$ is the fluctuating enthalpy per particle. Therefore, $\chi_T(Q,t)$ directly probes the correlations between the fluctuations of the single-particle density and that of the enthalpy. Using transformation from NPT to NPH ensemble and Equation 3.5, we have

$$\chi_4(Q,t) = \chi_4^{NPH}(Q,t) + \frac{k_B T^2}{c_P}\chi_T^2(Q,t) \geq \frac{k_B T^2}{c_P}\chi_T^2(Q,t) \tag{3.6}$$

This inequality can be used as equality at low temperatures.

3.2.4 Low temperature: fragile-to-strong

We study the dynamic response function $\chi_T(Q,t)$, of deeply supercooled water by means of Quasi-Elastic Neutron Scattering and Molecular Dynamics Simulations. Both techniques show an increase in the peak height of $\chi_T(Q,t)$ as the temperature is lowered toward the dynamic crossover temperature T_L. Below T_L, the peak height decreases steadily. We attribute this phenomenon to the change of slope of the Arrhenius plot of the translational relaxation time at T_L. In contrast, the peak height of the calculated four-point correlation function $\chi_4(Q,t)$, directly related to the size of dynamic heterogeneity, increases toward and below T_L.

The measured QENS spectrum is analyzed with the following stretched exponential model[95, 96, 98, 55, 54, 97, 36, 162, 90, 136, 134, 33, 67, 135, 16, 39, 40, 150], which has been tested extensively by MD simulations and QENS experiments. According to this model, the measured spectral intensity distribution is expressed as

$$I(Q,E) = N \cdot (f(Q) \cdot \delta(E) + (1 - f(Q)) \cdot \mathscr{F}\{F_s(Q,t)\}) \otimes R(Q,E) \tag{3.7}$$

where N is the normalization factor and $f(Q)$ is the elastic scattering component, that takes into account the contribution coming from hydrogen atoms that cannot migrate more than a distance $\sim 2\pi/Q$, within the experimental observation time window. $F_s(Q,t)$ is the self-intermediate scattering function (SISF) of the hydrogen atoms in the hydration water, $R(Q,E)$ is the Q-dependent energy resolution function as obtained by a low temperature run at 10 K using the hydrated sample.

A sum of four Gaussian functions was used to represent the $R(Q,E)$. Generally, the SISF is a product of the translational part, $F_T(Q,t)$, and the rotational part, $F_R(Q,t)$, i.e. $F_S(Q,t) = F_T(Q,t)F_R(Q,t)$. By using only the spectra with $Q < 1\text{Å}^{-1}$, the rotational contribution can be made negligibly small. So the SISF is modeled as

follows:

$$F_s(Q,t) \approx F_T(Q,t) = F^v(Q,t) \cdot \exp\Big[-\Big(\frac{t}{\tau(Q,T)}\Big)^{\beta}\Big] \tag{3.8}$$

where the first factor, $F^v(Q,t)$, represents the short-time vibrational motion of the water molecules in the cage. This factor affects the SISF in sub-ps time scale, thus is not an observable effect in this experiment (i.e. $F^v(Q,t) \approx 1$).

It is debatable whether the relaxation process we observed with QENS in supercooled confined water is the slowest relaxation of the system (α-relaxation). Nevertheless, it is verified by both experiments (Figure 3-2) and MD simulations (Figure 3-4a) that the relaxation process we observed obeys a stretched exponential decay. Since this is the only a priori assumption of the Relaxing Cage Model, our results are still interesting to report even if the major process is not the genuine α-process: the observation of a crossover is anyway a feature that is revealing some change in the structure of the hydrogen bond network.

Figure 3-2 shows two spectra taken above and below the crossover temperature. One should note from these two plots that the wing of the spectra is significantly larger than the resolution function. This is because the Fourier transform of the stretched exponential form of SISF produces a significantly wide skirt, and allows meaningful data analyses.

Figure 3-3(a) shows the experimentally extracted $\langle\tau\rangle$ as a function of $1/T$. A gradual transition (change of slope) from a super-Arrhenius at high temperatures (non-linear behavior) to an Arrhenius behavior at low temperatures (linear behavior) can be seen as the temperature is cooled down across T_L.[18, 79] To determine the dynamic crossover temperature T_L experimentally, we plotted the derivative of the Arrhenius plot, $d\ln\langle\tau\rangle/d(1/T)$ (Figure 3-3(b)). The peak, or equivalently the change of the slope in the Arrhenius plot, suggests that $T_L = 225 \pm 5$ K, in agreement with the peak position of the DSC data reported in Figure 3-3(d) ($T_L = 227 \pm 2$ K).

We are now going to show that it is possible to evaluate this crossover temperature also from the dynamic response function $\chi_T(Q,t)$. Figure 3-3(c) shows the dynamic

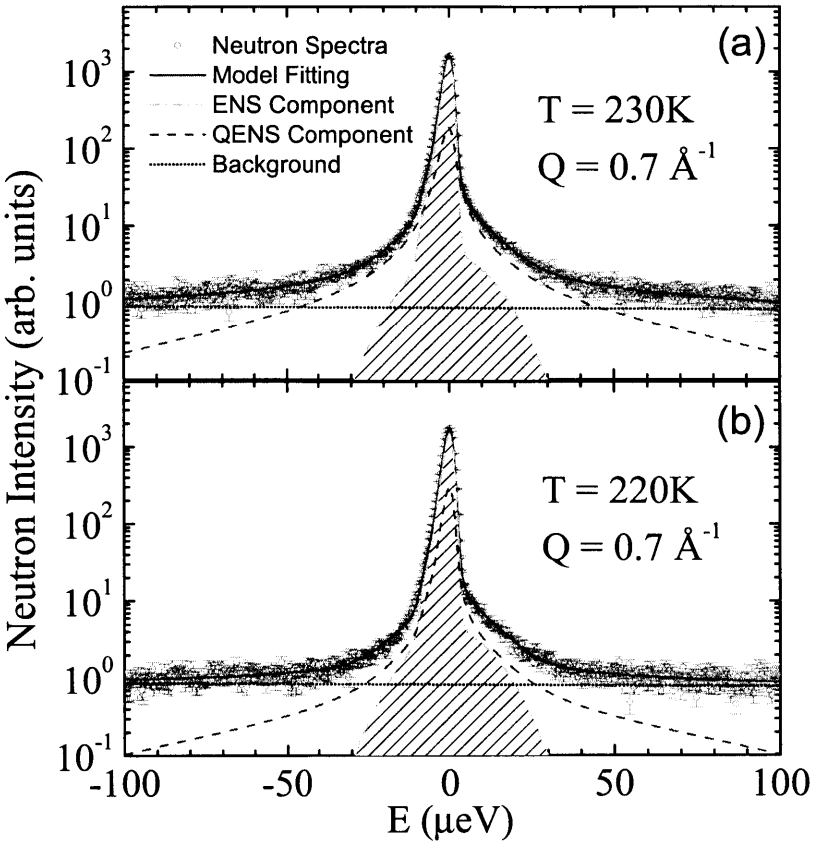

Figure 3-2: Illustration of the analysis of QENS spectra at two typical temperatures T = 230 K (a), 220 K (b) at Q = 0.7 Å^{-1}. The hollow circles are the measured neutron intensity as a function of the energy transfer E. The solid line is the fitted curve using the RCM model. The dash-dotted line with shadow is the elastic scattering component, whose asymmetric shape derives from the asymmetric Q-dependent resolution function. The dashed line is the quasi-elastic scattering component. The dotted line is the background.[163]

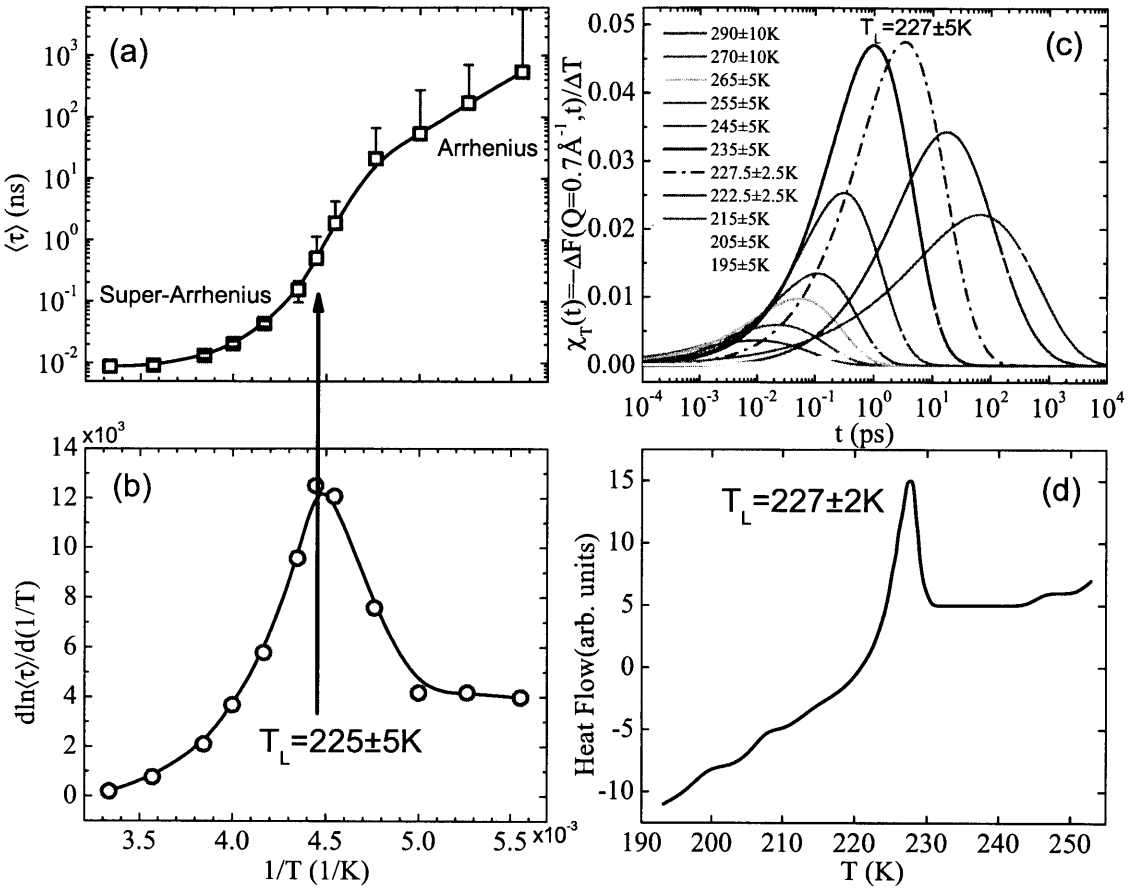

Figure 3-3: (a) Arrhenius plot of the experimental translational relaxation time for water confined in aged cement paste. (b) Derivative of the Arrhenius plot of the translational relaxation time. (c) Dynamic Susceptibility calculated with finite differences of the SISF. (d) DSC curve of water confined in 8-day-old hydrated cement paste.[163]

response function for several temperatures as a function of time. $\chi_T(Q,t)$ is calculated using finite differences. The peak height of $\chi_T(Q,t)$, $\chi_T^*(Q,t)$, grows as T is lowered and reaches a maximum at $T_L = 227 \pm 5$ K, but this growth is interrupted when the dynamic crossover sets in. The reason for this behavior is clear if one considers that,

$$\chi_T(Q,t) = -\frac{\partial F_s(Q,t)}{\partial T} = F_s(Q,t)\beta \left(\frac{t}{\tau(Q,T)}\right)^{\beta} \frac{\partial \ln \tau(Q,T)}{\partial(1/T)} T^{-2} \qquad (3.9)$$

The only parameter in $F_s(Q,t)$ that has to be differentiated with respect to T is $\tau(Q,T)$, since β remains almost constant and close to 0.5 $\pm$ 0.1 as T is lowered. $\chi_T^*(Q)$ is therefore directly proportional to the change of slope of the Arrhenius plot of $\tau(Q)$ (Figure 3-3(b)).

Therefore, the three quantities $\chi_T(Q,t)$, $\langle\tau\rangle$ and DSC heat flow all agree in evaluating the crossover temperature as $T_L \approx 225 \pm 5$ K. These experimental findings demonstrate that there are well-defined thermodynamic and dynamic signatures in the response functions of the existence of the crossover temperature, T_L. To make sure that these phenomena are inherent properties of water and not due to the confinement, we ran a simulation of a model bulk water, TIP4P-Ew. The dynamic crossover in the Arrhenius plot of the self-diffusion constant has been previously observed with simulations of bulk water using other water models.

We calculated long MD trajectories for a box of 512 water molecules of up to 1 μs in the NVT ensemble. The systems were considered equilibrated when the mean square displacement of the water molecules was larger than 0.1 nm^2 [30] (see Figure 3-4c). We then calculated the SISF for the oxygen atoms for 5 Q-values (0.4, 0.5, 0.6, 0.7, 0.8 Å^{-1}) and fit the data according to the model described above (see Figure 3-4a). Figure 3-4b and Figure 3-4d show the Arrhenius plots of the transport properties obtained from the trajectories: the translational relaxation time $\langle\tau\rangle$ and the inverse of the self-diffusion constant $1/D$, respectively. Both the plots show a dynamic crossover at $T_L = 215 \pm 5$ K, analogous to the one in Figure 3-3(a). As a side note, $\langle\tau(T_L)\rangle$ is between 1 to 10 ns range for both experiments and simulations, confirming the general behavior of many glass formers.

The upper panel of Figure 3-5 shows the dynamic response function $\chi_T(Q,t)$ extracted from the trajectories. Error bars on $\chi_T(Q,t)$ are of the order of 10^{-2} K^{-1}. As also observed experimentally, $\chi_T^*(Q)$ decreases after the dynamic crossover temperature $T_L = 215$ K.

The same phenomenon is not observed for $\chi_4(Q,t)$ calculated from the trajectory

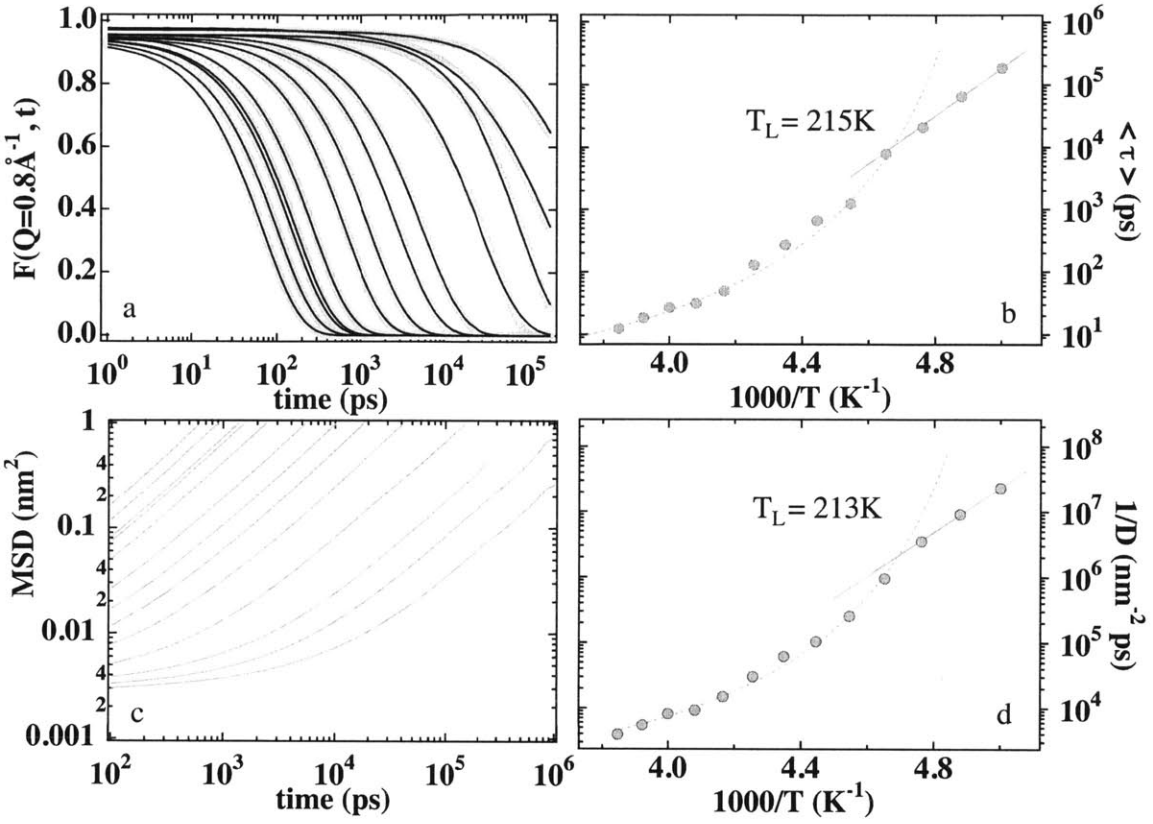

Figure 3-4: Simulation results. (a) Oxygen SISF at $Q = 0.8$ Å^{-1} for several temperatures (from 260 to 200 K, every 5 K). Continuous lines are the best fittings with RCM. (b) Arrhenius plot of the translational relaxation time. The dashed line is the fitting of the Vogel-Fulcher-Tammann (VFT) law, the solid line is the Arrhenius law. (c) long-time mean square displacement. (d) Arrhenius plot of the self-diffusion constant.[163]

(Figure 3-5, lower panel). Since $\chi_4(Q,t)$ is related to spontaneous fluctuations, its direct measurement is very difficult. Much easier way is the numerical computation.

The general features of $\chi_4(Q,t)$ for bulk water resemble the ones for Lennard-Jones systems. The power law dependences of the short time regime and the growth of the peak height of $\chi_4(Q,t)$ as one approaches T_L are evident. Comparing the two panels of Figure 3-5, one notices that while the $\chi_T(Q,t)$ peak height has a maximum at $T = T_L$, $\chi_4(Q,t)$ peak height keeps increasing even below T_L. This phenomenon may be understood by considering that these two quantities are related by the inequality.

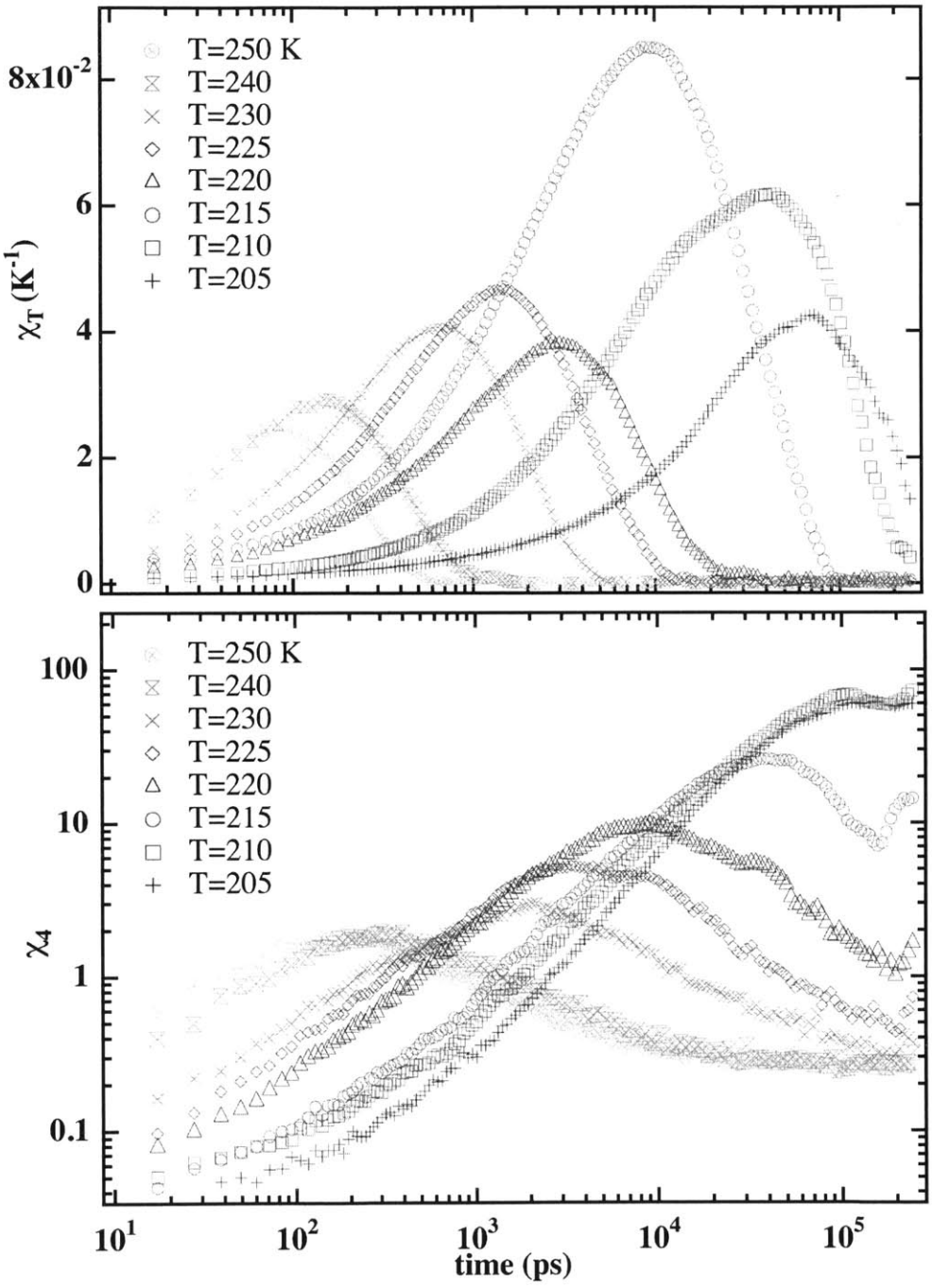

Figure 3-5: Upper Panel: Dynamic Susceptibility $\chi_T(Q,t)$ for TIP4P-Ew water at several temperatures, for $Q = 1.0$ Å^{-1}. Lower Panel: Log-log plot of $\chi_4(Q,t)$, for $Q = 1.0$ Å^{-1}.[163]

This inequality implies that since the specific heat of confined water has a peak at the dynamic crossover temperature, the dynamic susceptibility may decrease after T_L to keep $\chi_4(Q,t)$ growing.

In conclusion, we showed that bulk water simulations are able to reproduce our experimental findings of the 3-D confined water. The maximum of $\chi_T^*(Q)$ happens at the dynamic crossover temperature T_L and it is not originated from the confinement. On the other hand, the peak height of $\chi_4(Q,t)$, which is a measure of the dynamic heterogeneity, continue to increase below T_L.

3.2.5 High temperature: strong-to-fragile

The diffusive dynamics of hydration water in lysozyme is studied by high-resolution incoherent quasi-elastic neutron scattering (QENS) spectroscopy and molecular dynamics (MD) simulations in a temperature range of 290 K $< T <$ 380 K. The hydration level of the protein powder sample is kept at $h = 0.35$ gram of water per gram of dry protein to provide monolayer of water coverage on the protein surfaces. Two lysozyme samples, the H_2O hydrated and the D_2O hydrated, are measured in the experiments. The difference spectra of the two are used to extract the diffusive dynamics of the hydration water. The self-diffusion constant D of the hydration water is obtained from analyses of the low-Q spectra. The Arrhenius plot of the inverse diffusion constant (i.e. $\log(1/D)$ vs. $1/T$) shows a dynamic crossover from a Super-Arrhenius behavior at low temperatures to an Arrhenius behavior at high temperatures bordered at $T_D = 345 \pm 5$ K. We also observe a pronounced increase of the migration distance d of the hydration water molecules above T_D. We present evidence from the neutron scattering experiment that this dynamic crossover temperature in the hydration water coincides with that of the reversible denaturation of lysozyme determined by specific heat measurements. We further performed MD simulations of hydrated lysozyme powder to offer a plausible reason for this coincidence of the crossover phenomenon with the reversible denaturation of the protein.

Lysozyme, a small globular protein of 129 amino acid residues, exhibits intermediate structures under chemical denaturation, pressure-induced denaturation and thermal denaturation. Its unfolding process can therefore be considered as a three-state model $N \rightleftharpoons I \rightarrow U$. The first step is usually called reversible denaturation and can be seen as a kind of strong-to-fragile liquid transition associated with the configurational entropy change, while the second step is the irreversible denaturation and it is due to an association of unfolded lysozyme units. These experimental findings have been confirmed by theory and simulation.

We suggest that this reversible denaturation is probably related to the dynamic crossover that protein hydration water undergoes at $T_D \approx 345 \pm 5$ K. At this temperature, a sudden change in hydration water dynamics takes place, the inverse diffusion constant switches from a Super-Arrhenius behavior at low temperatures to an Arrhenius behavior at high temperatures. Neutron scattering has been used to study the dynamics of hydration water at room temperatures, in solutions, at different hydration levels. A previous NMR investigation of the long-time diffusion of the hydration water in lysozyme has detected the existence of both a high and a low temperature dynamic crossover phenomena. NMR measures long time (milli-second) diffusion constant, during which the water molecules may have reached the boundary of the confinement and reflected back, while QENS measures at sub-nanosecond scale, so the self-diffusion constant D measured by QENS is more accurate. We also extracted the migration distance d of the hydration water molecules from QENS and observed that d showed a pronounced increase about T_D, which has not been reported in the NMR experiments.

The existence of these phenomena can also be shown theoretically. In fact whenever the specific heat has a peak, the Arrhenius Plot of the inverse of the diffusion constant has a slope change. This can be seen with the Adam-Gibbs equation,

$$\frac{1}{D} = \frac{1}{D_0} \exp\left(\frac{C}{TS_{conf}}\right) \tag{3.10}$$

where $1/D_0$ is a prefactor, C is a constant and S_{conf} is the configurational entropy. If we assume that the Adam-Gibbs equation is valid also at high temperatures for hydration water, the specific heat peak recently observed by calorimetry during lysozyme thermal denaturation by Salvetti et al. [129] (Figure 3-6(A)) suggests the existence of a high-temperature crossover phenomenon for the inverse of the diffusion constant. These results were confirmed by Mallamace et al. with NMR measurements. They also found that the contribution of the configurational disorder to entropy is dominant, so $S_{conf} \approx S$ and

$$S_{conf}(T) \approx S_{conf}(0) + \int_0^T \frac{c_P}{T} dT \tag{3.11}$$

This law has been found to be valid at low temperature in the supercooled region of water by computer simulations and to a certain extent by experiments. As a numerical example, the Arrhenius plot of the resulting $D0/D$ as obtained by substitution of c_p reported in [129] is shown in Figure 3-6(B). Both the plots of entropy and D0/D have a kink at 340 $\pm$ 5 K, corresponding approximately to the maximum in the specific heat.

The inverse diffusion constant 1/D and the migration distance d of the hydration water molecules are extracted from our QENS spectra. The inverse diffusion constant $1/D$ (to compare with QENS result), the protein backbone RMSD, hydrogen bond relaxation time τ_R and protein hydrogen atom mean square displacement $\langle x^2 \rangle$, are calculated from MD simulations[89]. These quantities taken all together indicate that an abrupt change in the water-lysozyme hydrogen bonding occurs in the temperature interval between 330 K and 345 K, in the same temperature range found by calorimetric and Raman scattering measurements5,6 for the reversible conversion of $N \rightleftharpoons I$ in lysozyme solutions.

An analogous dynamic crossover in the inverse diffusion constant has been previously found experimentally for protein hydration water at much lower temperatures

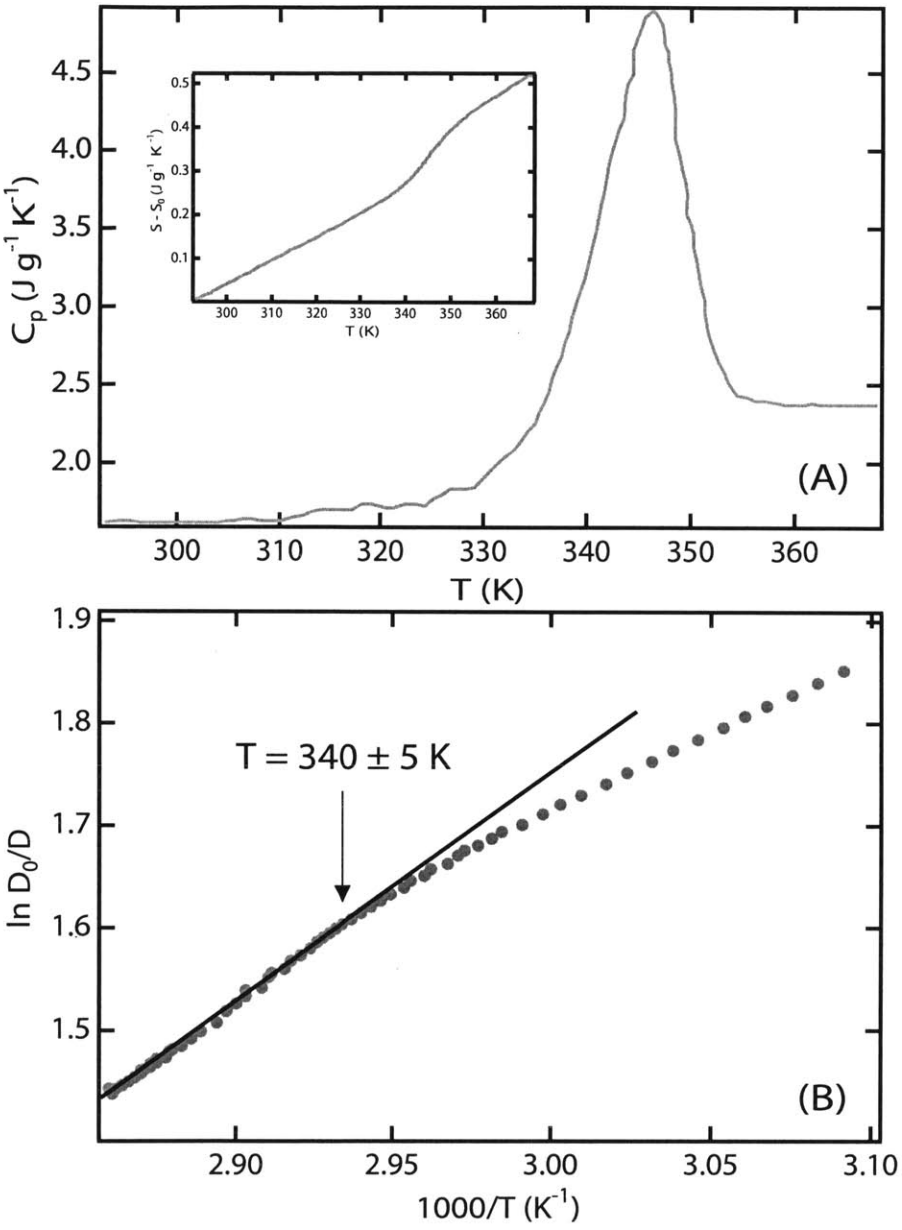

Figure 3-6: (A) Specific heat measurement of lysozyme solution. Inset: Entropy as a function of temperature, calculated from integration of the experimental c_P, from 290 K to 370 K. (B) Arrhenius Plot of D_0/D vs. $1000/T$, calculated according to the Adam-Gibbs equation. D_0 is the prefactor in the Adam-Gibbs equation, S_0 is $S(290K)$. As a numerical example, we chose $S_0 = 1$ J/gK and $C = 700$ J/g. This equation predicts a change in the slope for the inverse of the diffusion constant at 340 ± 5 K.[164]

(T_L 220 K), where another peak in the specific heat takes place. This was attributed by an MD simulation to the crossing of the Widom line of the hydration water[146, 158, 38, 37]. The corresponding crossover for the average α-relaxation time defined using the Relaxing Cage Model found in experiments has been recently confirmed by an MD simulation using the same powder protein model used in this paper[89]. This low temperature crossover T_L was shown to coincide with the so-called dynamic transition temperature of the protein.

Following the protein powder model developed by Tarek and Tobias, we put in a box two OPLS-AA29 lysozyme molecules (Protein Data Bank file 1AKI.pdb) randomly oriented and 484 TIP4P-Ew water molecules, thus $h = 0.3$ for each protein. Eight chloride ions for each protein were added to neutralize the system, composed of 5872 atoms. The Lennard-Jones interactions were truncated beyond 1.4 nm, while electrostatic interactions, calculated with the Particle Mesh Ewald method were truncated at 0.9 nm. Three-dimensional periodic boundary conditions were applied and the equations of motions were integrated using the Verlet leap-frog algorithm with a 2 fs time step. All bonds were constrained at their equilibrium values using the LINear Constraint Solver algorithm32 (LINCS). After an energy minimization of 5000 steps with the Steepest Descent algorithm, we equilibrated the system in a NPT ensemble (isobaric-isothermal) for 10 ns at 300 K. We performed 9 simulations at different temperatures (from 290 K to 370 K, with 10 K intervals) with a parallel-compiled version of GROMACS33. Simulations were performed using a triclinic cell (box size $\sim$ 43 Å$\times$ 37 Å$\times$ 32 Å) and each MD simulation length was 50 ns after the equilibration time.

The hydrogen bond correlation function[102] was calculated according to

$$c(t) = \frac{\langle h(0)h(t)\rangle}{\langle h(t)\rangle} \tag{3.12}$$

where $h(t) = 1$ if the hydrogen bond exists and $h(t) = 0$ otherwise. From the decay

of this correlation function we can calculate the hydrogen bond relaxation time τ_R, as the 1/e value of $c(t)$.

The model discussed in [164] is used to analyze measured QENS spectra of the protein hydration water for temperatures ranging from 290 K to 380 K, covering the first stage of the denaturation process, occurring at the reversible protein denaturation temperature around 345 K. By using only the spectra with $Q \leq 1$ Å^{-1} (i.e. $Q = 0.37$, 0.73, 1.07 Å^{-1}), where Q denotes the magnitude of the scattering vector, we can approximate the incoherent dynamic structure factor for the hydrogen atoms by a Lorentzian. Using this model, the spectra measured at all temperatures and wave vector transfers can be fitted well in the whole energy transfer range -200 μeV ¡ E ¡ 200 μeV. The analysis result indicates that the factor $p(Q)$ takes a value of 0.54. This means that 46% of the spectral area is contributed from the hydration water that is free to diffuse in the time window of the spectrometer. The asymmetry of the spectra can be accounted for very well by allowing for an asymmetric shaped energy resolution function. We can use this model to extract the Lorentzian shape spectrum, coming from the diffusive motions of protein hydration water, having a Q-dependent line width $\Gamma(Q)$ with a good accuracy. The good agreement between the fitted curve and the measured intensity shows the validity of the model.

Figure 3-7 shows the Arrhenius plot of the extracted $\log(1/D)$ vs. $1/T$ and d vs. T from this model. Figure 3-7(A) shows an evidence of an Arrhenius to Super-Arrhenius dynamic crossover as the temperature is raised across $T_D = 345 \pm 5$ K. Below T_D, the inverse diffusion constant can be fitted with the Vogel-Fucher-Tamman Law as $1/D = 1/D_0 \exp(CT_0/T - T_0)$ with $T_0 = 204 \pm 36$ K and $C = 0.94$. While above T_D, the inverse diffusion constant can be fitted with the Arrhenius Law $1/D = 1/D_0 \exp(E_A/RT)$ with $E_A = 5.97 \pm 0.55$ kcal/mol, which corresponds to about an energy needed to break 2.4 hydrogen bonds at T_D. The exact value of T_D is then evaluated as the crossing point of the two laws. Figure 3-7(B) shows the extracted d, which represents the migration distance of the water molecules between two successive

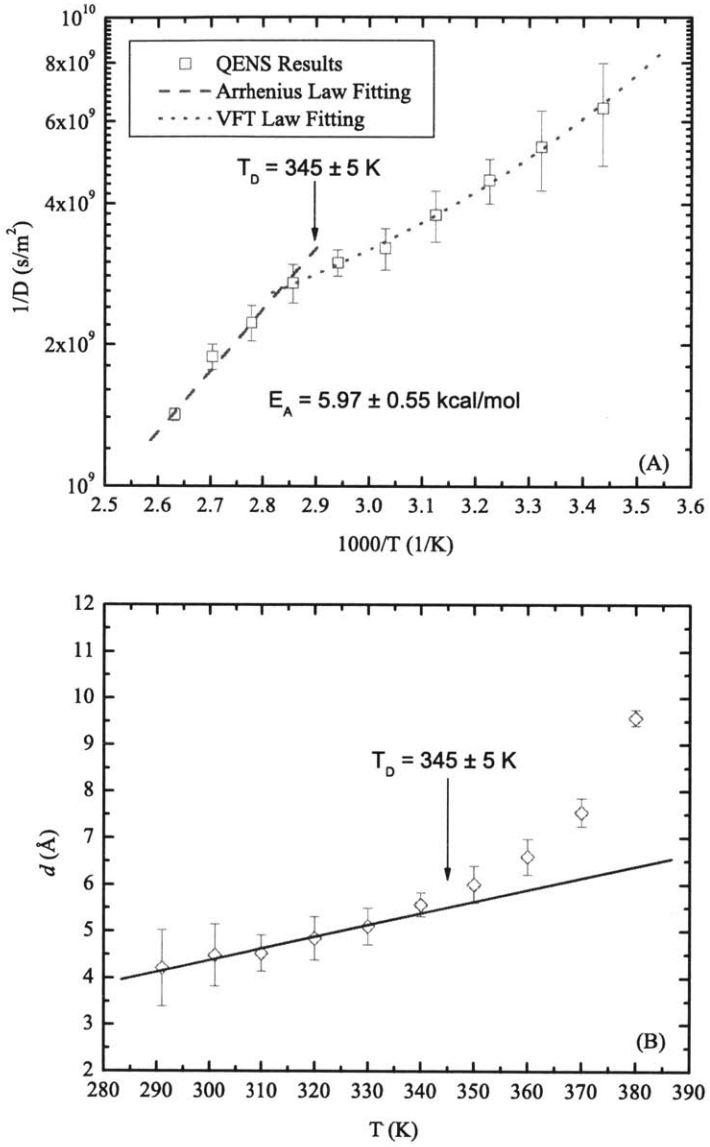

Figure 3-7: (A) Arrhenius Plot of experimentally extracted $\log(1/D)$ vs. $1000/T$ of the protein hydration water shows an evidence of an Super-Arrhenius (non-linear behavior) to Arrhenius (linear behavior) dynamic crossover as the temperature is raised through $T_D = 345 \pm 5$ K. (B) Plot of experimentally extracted average migration distance d of the hydration water. This quantity is slowly increasing linearly within experimental error bars below T_D, but rises sharply above T_D, indicating a longer migration of water molecules in-between two successive trap sites.[164]

trap sites. One can see that it is increasing slowly below T_D, from 4.2 to 5.6 Å, but rises sharply above T_D to 9.6 Åat 380 K. The result is consistent with the previous

results 6 9 Åat room temperature. The sharp changes of both the self-diffusion constant D and the migration distance d indicate a large scale enhanced movement of the water molecules above T_D, when the lifetime of the hydrogen bonded network of the water molecules becomes shorter, and thus it is not able to maintain the shape of the protein. The following MD simulation results confirm this dynamic crossover and further show that the dynamic crossover in protein hydration water is probably connected to the first stage of the unfolding process of the protein.

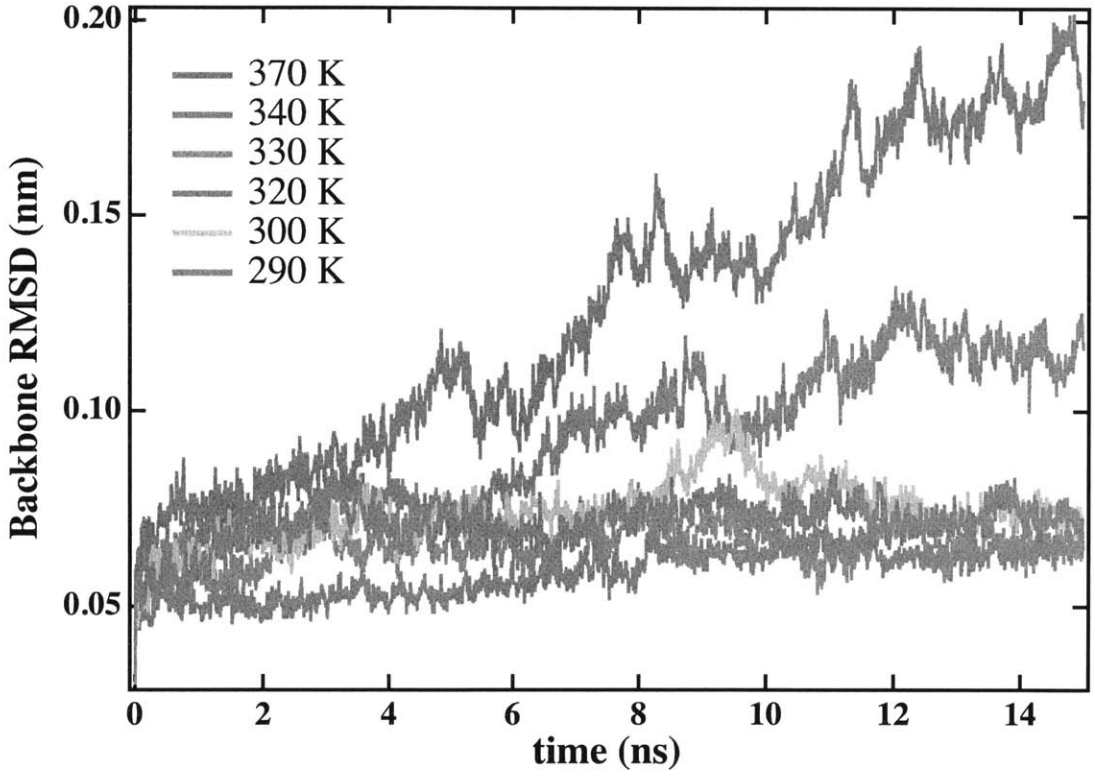

Figure 3-8: Comparison of the Backbone RMSD as a function of time at different temperatures. This quantity was calculated for the last 15 ns of the trajectories and averaged over the two lysozyme molecules. No remarkable change is detected until 340 K, when the protein increases its flexibility. Although the simulations are too short to follow the whole denaturation process, they are still able to capture its beginning. [164]

The protein backbone RMSD calculated from the trajectories shows a sudden

increase between 330 K and 340 K (Figure 3-8), signaling the beginning of the denaturation process. Molecular Dynamics simulations are limited to a timestep on the order of fs, while protein unfolding occurs on timescales of the order of ms. Therefore, atomistic simulations of the whole denaturation process are still utopian for the conventional computers capabilities. Nevertheless, a few ns are enough to capture at least its dynamic beginning.

At the same temperature, the Arrhenius plot of $1/D$ obtained from the MD simulation shows a change in its behavior at $T_D = 340 \pm 5$ K, reproducing well the neutron scattering data and qualitatively the Adam-Gibbs equation. In particular, the extracted activation energy $E_A = 5.25 \pm 0.5$ kcal/mol is in agreement with the experimental value ($E_A = 5.97 \pm 0.55$ kcal/mol).

The underlying physical mechanism for lysozyme reversible denaturation can be seen from examination of the following three physical quantities calculated from the MD simulations. Figure 3-9(A) displays the onset temperature of the reversible denaturation, T_D: the protein hydrogen atoms MSD has a sharp increase as a function of temperature between 330 K and 340 K, in agreement with the onset temperature for reversible denaturation determined by calorimetry.

Figure 3-9(B) shows that at the same temperature T_D, the inverse of the water-protein hydrogen bond relaxation time (relaxation rate) deviates from linearity, signaling the beginning of the breakdown of the hydrogen bond network around the protein. The increase in the hydrogen bond relaxation rate is therefore the cause of the enhanced protein flexibility, as already pointed out by Wood et al. for the low temperature protein dynamical transition. In that case, they found a correlation between the decrease of protein H-bond network relaxation time (due to the onset of water translational diffusion) and the sudden increase in the protein hydrogen atoms MSD at $T_L = 220$K. The situation is qualitatively analogous for the high temperature case, but with a quantitative difference: the solvent cage is not able to constrain the folded protein structure anymore and the macromolecule increases its ability of sam-

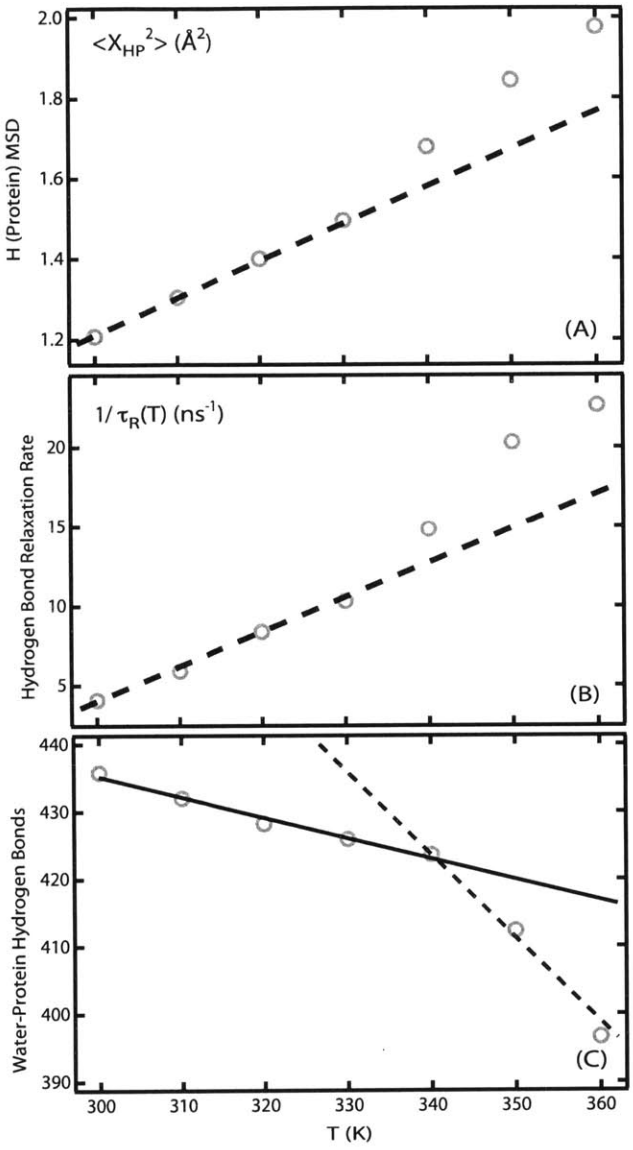

Figure 3-9: Arrhenius plot of the inverse diffusion constant for lysozyme hydration water, 1/D vs. 1000/T, calculated from MD simulations. The curve shows an Arrhenius (high T) to Super-Arrhenius (low T) dynamic crossover similar to the one observed by Quasi-Elastic Neutron Scattering (see Fig. 6). The diffusion constant has been calculated from the trajectories according to the Einstein relation, with a linear fit of water MSD from 300 to 600 ps. Numerical data are fitted with a Vogel-Fulcher-Tammann law at low temperatures (dashed line) and with an Arrhenius law at high temperatures (solid line).[164]

pling the configurational space. Due to the decrease of the hydrogen bond lifetime, its flexibility becomes large enough to start the unfolding process.

Figure 3-9(C) shows that as T further increases, the number of hydrogen bonds between water and the protein has a sharp change in its rate of decrease at $T_D = 340$ K, from 0.3 to 1.2 H-bonds/K. That is to say, the dynamics of interfacial water and its interactions with the protein surface are critical for the stability of protein structure. As soon as the strength of H-bonds at the interface between water and protein reaches a certain value, the 2-D network around the protein that kept it folded collapses, allowing the macromolecule to increase its flexibility and to begin the denaturation process. We believe that the crossover phenomenon is a characteristic of the whole water-protein system: the decreased interaction at the water-protein interface is the cause of both the crossover and the denaturation. On one hand, water becomes more mobile (increased diffusion constant); on the other, protein is not constrained by the hydrogen bond network and can unfold.

We show experimentally that: (1) the low-Q QENS data follows very well the simple model and we can thus extract the temperature dependence of the self-diffusion constant of protein hydration water with confidence; (2) the Arrhenius plot of the extracted inverse diffusion constant, $\log(1/D)$ vs. $1/T$, shows a Super-Arrhenius behavior at low temperatures and switches over to Arrhenius behavior at high temperatures bordering at $T_D = 345 \pm 5$ K; (3) we find a sudden increase of the average migration distance between two successive trap sites above T_D from the plot of d vs. T.

We show next that the MD simulation results generally complement and support the neutron scattering experimental findings. Specifically, (1) the Arrhenius plot of 1/D shows a break at the same crossover temperature $T_D = 340 \pm 5$ K and (2) the reversible denaturation phenomenon coincides with a sudden decrease of the lifetime of hydrogen bonds between hydration water and protein. We cannot conclude whether the denaturation of the protein and the dynamic crossover in its hydration water are

causally related, but their coincidence may suggest that the dynamic crossover could be a factor involved in the reversible denaturation process.

3.3 Fast dynamics

3.3.1 Inelastic neutron scattering

In an inelastic neutron scattering (INS) experiment, both the momentum transfer Q and the energy transfer E are measured. Strictly speaking, all neutron scattering processes are inelastic because of the existence of all kinds of atomic motions. The so-called elastic scattering just means to detect neutrons without analyzing the energy transfer E. By carefully analyzing the energy transfer, one can study how particles move. The characteristic dynamic response time and the energy transfer are approximately a Fourier pair. So the fast dynamics of water particles is represented at relatively high energy transfer range.

The Disk Chopper Spectrometer (DCS) at NIST Center for Neutron Research (NCNR) is a typical time-of-flight spectrometer. We use DCS to study picosecond-scale excess phonon density of state (boson peak) of water confined in MCM-41-S. DCS can be operated in many different modes so that a broad range of problems can be tackled with the right choice of mode. Using neutrons of incident energy of 16 meV, we obtain an elastic energy resolution of 1 meV, enough to study the inelastic peak at around 3-5 meV.

The Filter Analyzer Neutron Spectrometer (FANS) at NIST Center for Neutron Research (NCNR) is used to study the librational density of state of water confined in MCM-41-S. The design of FANS is similar to a triple-axis spectrometer. Instead of using an crystal analyzer, FANS uses a low-pass Bragg cutoff filter. Inelastic spectra are recorded by scanning the incident energy and detecting all scattered neutrons with energy $E_f < E_{cutoff}$. It is capable of varying incident neutron energies from 5 to 250 meV.

3.3.2 Boson peak

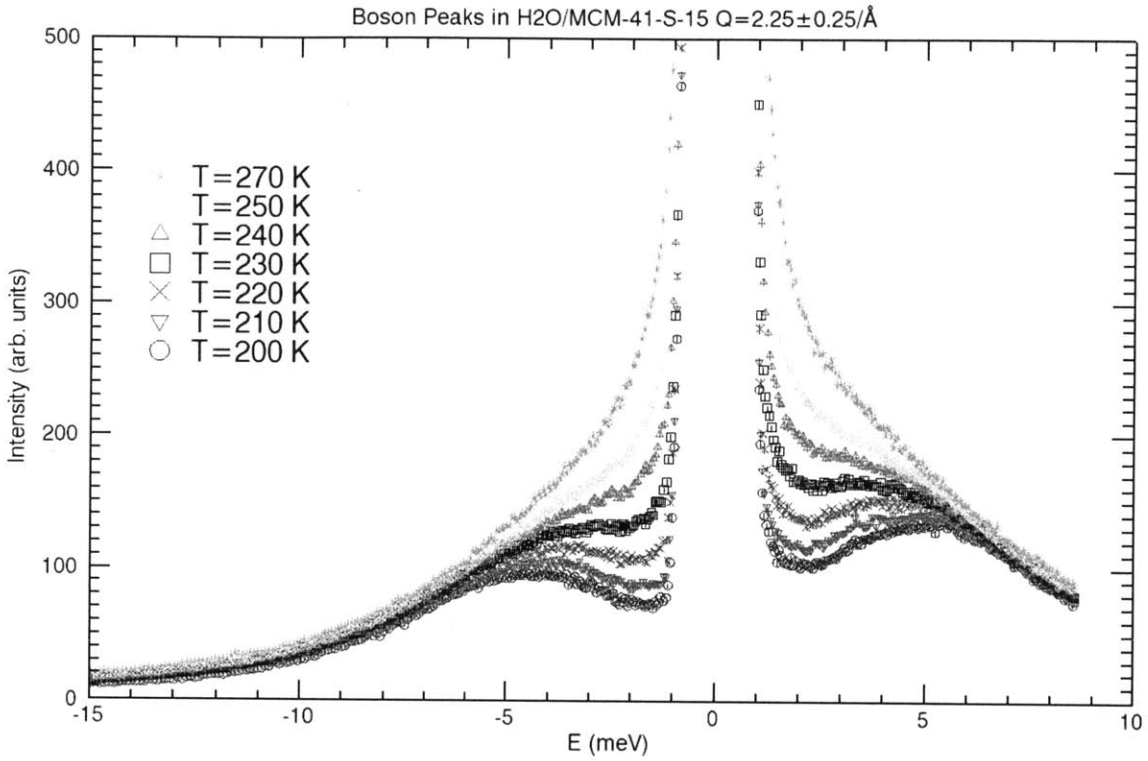

Figure 3-10: Boson peak of H_2O confined in MCM-41-S

Figure 3-10 shows the incoherent inelastic neutron scattering (INS) spectra of water confined in MCM-41-S. It can be seen on the temperature dependence of the INS spectra that a well-defined Boson peak[133, 131, 73, 71, 132, 77, 139, 137, 138, 62, 116, 121] at 5 meV appears at and below $T_L = 230 \pm 5$ K. Based on the previous interpretation of Widom line and its associated second critical point of water in the deeply supercooled region, the local structure of supercooled water transforms from predominantly a high-density liquid (HDL) to a low-density liquid (LDL) form at the dynamic crossover temperature T_L[87]. From neutron diffraction experiment, the HDL does not have a well-defined tetrahedral hydrogen bond structure (a fragile liquid), while LDL has an ice-like fully developed tetrahedral hydrogen bond structure (a strong liquid). Our experimental results imply that in LDL the cage effect becomes

more important because of the fully developed random tetrahedral hydrogen bond network (RTN). Therefore, the activated hopping process takes longer time to develop, leaving enough time for the in-cage vibration. One should notice that this kind of vibration is highly anharmonic because of the disordered nature of the RTN. It is well established in the literature that in Raman scattering a well-defined Boson peak appears in a glassy liquid which is classified as "strong". On the other hand, there is no discernable Boson peak in a glassy liquid which is classified as "fragile". Our measurement of the temperature dependence of Boson peak indicates a decrease of the fragility as temperature is lowered. The result gives the additional evidence that T_L marks a fragile-to-strong crossover. How the short time dynamics relates to the long time stretched exponential relaxation awaits for further investigation.

3.3.3 Density of states

In order to confirm the existence of the first-order liquid-liquid phase transition of water discussed in Chapter 2, we further performed FANS measurements of the librational density of states $G(E)$ of H_2O confined in MCM-41-S. The experimental procedure is similar to the detection of the density hysteresis. We performed two experiments on the same sample. In the first experiment, the hydrated sample is pressurized at room temperature to 2500 bar, and then cooled down to 180 K. In the second experiment, the hydrated sample is first cooled down to 130 K, and then pressurized to 2500 bar, and then warmed up to 180 K. So both of the experiments are performed at the same temperature and the same pressure. The temperature-dependent pressure is corrected for the two experiments. The only difference of the two experiments are the preparing path in the phase diagram.

Figure 3-11 shows the measured librational density of states $G(E)$ of H_2O confined in MCM-41-S. First, this experiment confirmed that the confined water at this phase point is still in liquid state. The librational density of sates of ice Ih exhibits much sharper increase in the energy range from 60 to 70 meV. So the previously measured

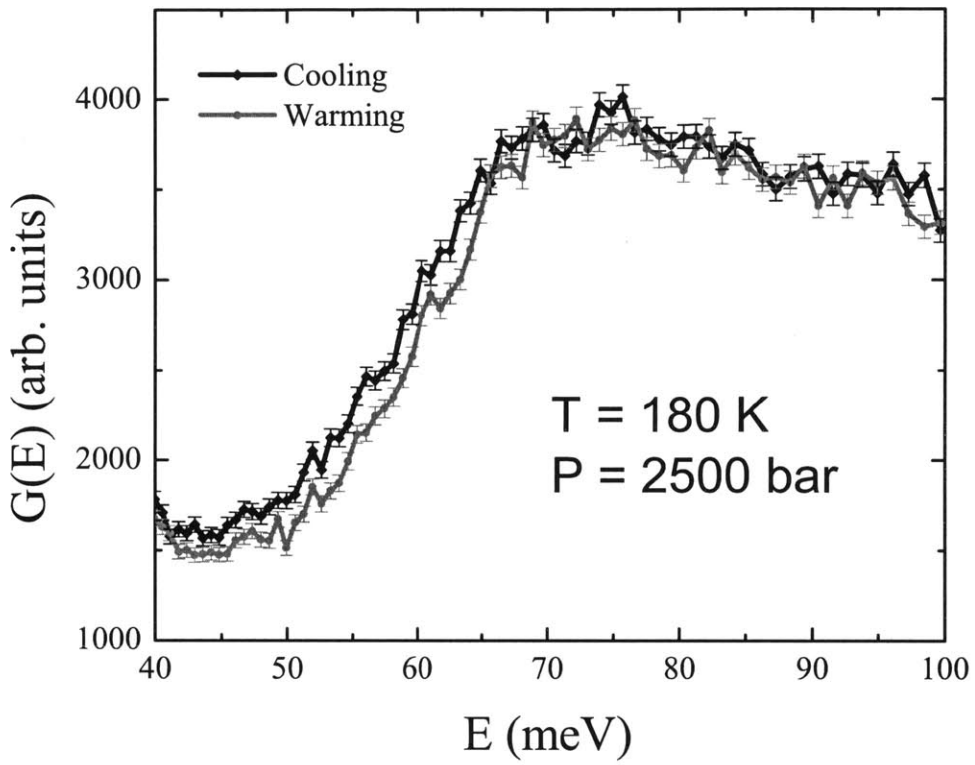

Figure 3-11: Librational density of states $G(E)$ of H_2O confined in MCM-41-S

density hysteresis is not likely due to the ice formation, either inside or outside the pores.

Furthermore, one can clearly see that the difference between the two $G(E)$ is beyond the error bars, although both measurements are performed at 180 K, 2500 bar. The difference might be explained as an evidence of crossing the first-order phase transition line. Therefore, the water in the sample prepared by cooling could be dominated by HDL, while the water in the sample prepared by warming could be dominated by LDL.

3.4 Universal pre-glass-transition temperature

In this chapter, using different neutron scattering techniques, we have experimentally detected several pre-glass-transition phenomena. They seem to occur at a universal pre-glass-transition temperature $T_{pg} \approx 225$ K, which is higher than the conventional glass-transition temperature T_g of water. The glass-transition temperature is practically defined as the temperature when the viscosity reaches 10^{12} Pa·s or the relaxation time reaches 100 s. In the case of water, the glass-transition is so week that the actual glass-transition temperature of water is still under debate[70, 161, 155]. However, above the glass-transition temperature, many pre-glass-transition phenomena already occur, including, but are not limited to, a fragile-to-strong dynamic crossover, an enhanced dynamic heterogeneity and the appearance of a well-defined boson peak. The Stokes-Einstein relation also breaks down at this pre-glass-transition temperature T_g.

Interesting enough, the temperature of the change of dynamical behavior at around $T_{pg} \approx 225$ K for H_2O happens to be the same as that of the peak of the specific heat[119, 105], and is fairly close to the peak of the thermal expansion coefficient of confined D_2O at 244 K[1]. The coincidence reveals the underlying correlation between the dynamic anomalies and thermodynamic anomalies[144, 148]. It may be possible that the link comes from the crossing the Widom line[60, 86, 158] emanating from the liquid-liquid critical point of water, which further originates from the two-length scale interaction potential of water[27, 59]. It may also be possible that it is due to a second-order phase transition, then the liquid-liquid critical point is in fact a tricritical point.

On the other hand, these phenomena can be well reproduced by the extended mode-coupling theory with an hopping effect incorporated[66, 43]. The extended mode-coupling theory doesn't need to invoke a critical point a high pressure. And it is applicable to general glass-forming liquids. A wide range of similar pre-glass-transition phenomena are also reported. Therefore, it is logical to ask how different

[1]The difference might be simply an isotopic effect.

is water from other glass-forming liquids.

Chapter 4

Summary and outlook

Man in Black: "They come, they fight, they destroy, they corrupt. It always ends the same." Jacob: "It only ends once. Anything that happens before that is just progress."

— Lost

4.1 Towards a unified theory of water

Water's unusual phase behavior has been an enduring mystery for centuries, challenging the deepest thinkers in every generation. The key to understand water's mysteries is the way water molecules interact with one another. The hydrogen bonds linking different water molecules are weaker than the covalent bonds holding hydrogen and oxygen atoms together, and are stronger than the van der Walls interaction. So the continuously breaking and reforming hydrogen bonds in water can form open tetrahedral structures, giving rise to many anomalous properties of water.

However, knowing the rules doesn't mean understanding the game. In a complex system like water, many counterintuitive emergent patterns arise out of the relatively simple interactions. The situation utterly resembles a child playing Go[1]. The new

[1]A game known as Wei Qi in Chinese.

findings of confined water reveal a deeper connection between the thermodynamic and dynamic properties of water. They may eventually stimulate new ideas towards a unified theory of water.

4.2 Randomness and emergence

The study of collective phenomena is and will remain one of the main intellectual challenges for a long time. Molecular theories can predict the macroscopic behaviors of many simple systems and processes from first principles. However, the behaviors of associated matters, strongly or weekly correlated, are so much more complex that methods of interpretation are cruder. Such systems range from turbulent fluids, amorphous solids and glasses, to innumerable examples in soft condensed matters (polymers, colloids, proteins, etc), where cooperativity and complex hierarchical structures are common and intrinsic.

In a deterministic world, the predictability is merely constrained by the computation power, so randomness is just an illusion. Every event is simply following its predetermined path. Fortunately, quantum mechanics restores the randomness and therefore leaves space for free will, unless certain hidden variables exit. Despite of the origin of randomness, it is human beings' instinct to quest for the novel emergent behaviors in the apparently random systems. The real question is: if such a law exits, does it apply to us?

Appendix A

A List of Publications

[1] **Yang Zhang**, Antonio Faraone, William A. Kamitakahara, Kao-Hsiang Liu, Chung-Yuan Mou, Juscelino B. Leao, Sung Chang and Sow-Hsin Chen, "Equation of States of Nanoconfined Water", to be published (2010).

[2] Cheng-Si Tsao, Yun Liu, Mingda Li, **Yang Zhang**, Juscelino B Leao, Wei-Shan Chiang, Tsui-Yun Chung, Yi-Ren Tzeng, Ming-Sheng Yu and Sow-Hsin Chen,"Probing the Room-temperature Spatial Distribution of Hydrogen in Nanoporous Carbon by use of Small-angle Neutron Scatterin", to be published (2010).

[3] Cheng-Si Tsao, Yun Liu, Mingda Li, **Yang Zhang**, Juscelino B Leao, Hua-Wen Chang, Ming-Sheng Yu and Sow-Hsin Chen, "Neutron scattering methodology for absolute measurement of room-temperature hydrogen storage capacity and evidence for spillover effect in a Pt-doped activated carbon", J. Phys. Chem. Lett. 1, 1569 (2010).

- Highlighted on the MRS website ACNS 2010.

[4] Sow-Hsin Chen, Marco Lagi, Xiang-qiang Chu, **Yang Zhang**, Chansoo Kim, Antonio Faraone, Emiliano Fratini and Piero Baglioni, "Dynamics of a globular protein and its hydration water studied by neutron scattering and MD

simulations", Spectroscopy: Biomedical Applications 24, 1 (2010)

- Highlighted on the cover of Spectroscopy: Biomedical Applications.

[5] Sow-Hsin Chen, **Yang Zhang**, Marco Lagi, Xiang-qiang Chu, Li Liu, Antonio Faraone, Emiliano Fratini and Piero Baglioni, "The dynamic response function $\chi_T(Q,t)$ of confined supercooled water and its relation to the dynamic crossover phenomenon", Zeitschrift für Physikalische Chemie 224, 109 (2010).

[6] Sow-Hsin Chen, **Yang Zhang**, Marco Lagi, Song-Ho Chong, Piero Baglioni and Francesco Mallamce, "Evidence of dynamic crossover phenomena in water and other glass-forming liquids: experiments, MD simulations and theory", J. of Phys.:Condens. Matter 21, 504102 (2009).

- Selected on Institute of Physics (IOP) Select.

[7] Sow-Hsin Chen, Xiang-qiang Chu, Marco Lagi, Chansoo Kim, **Yang Zhang**, Antonio Faraone, Juscelino B. Leao, Emiliano Fratini, Piero Baglioni and Francesco Mallamace, "Dynamical coupling between a globular protein and its hydration water studied by neutron scattering and MD simulation", Proceedings of WPI-AIMR (2009).

[8] **Yang Zhang**, Marco Lagi, Emiliano Fratini, Piero Baglioni, Eugene Mamontov and Sow-Hsin Chen, "Dynamic susceptibility of supercooled water and its relation to the dynamic crossover phenomenon", Phys. Rev. E 79, 040201 (2009).

- Selected on Virtual Journal of Biological Physics Research, Vol. 17, Issue 8 (2009).

[9] Antonio Faraone, **Yang Zhang**, Kao-Hsiang Liu, Chung-Yuan Mou and Sow-Hsin Chen, "Single particle dynamics of water confined in a hydrophobically

modified MCM-41-S nanoporous matrix", J. of Chem. Phys. 130, 134512 (2009).

- Selected on Virtual Journal of Biological Physics Research, Vol. 17, Issue 8 (2009).
- "Water dynamics in hydrophobic confinement", Highlighted on 2009 Accomplishments and Opportunities, NIST Center for Neutron Research, (2009).

[10] **Yang Zhang**, Marco Lagi, Dazhi Liu, Francesco Mallamace, Emiliano Fratini, Piero Baglioni, Eugene Mamontov, Mark Hagen and Sow-Hsin Chen, "Observation of high-temperature dynamic crossover in protein hydration water and its relation to reversible denaturation of lysozyme", J. of Chem. Phys. 130, 13501 (2009).

- Selected on Virtual Journal of Biological Physics Research, Vol 17, Issue 8 (2009).

[11] **Yang Zhang**, Kao-Hsiang Liu, Marco Lagi, Dazhi Liu, Kenneth C. Littrell, Chung-Yuan Mou and Sow-Hsin Chen, "Absence of the density minimum of supercooled water in hydrophobic confinement", J. of Phys. Chem. B 113, 5007 (2009).

[12] **Yang Zhang**, Marco Lagi, Francesca Ridi, Emiliano Fratini, Piero Baglioni, Eugene Mamontov and Sow-Hsin Chen, "Observation of dynamic crossover and dynamic heterogeneity in hydration water confined in aged cement paste", J. of Phys.: Condens. Matter 20, 502101 (2008).

- IOP journals 10% articles, accessed over 250 times in the first month of publication.
- IOP journals 3% articles, accessed over 500 times in the first year of publication.

- Selected on Institute of Physics (IOP) Select.

[13] Dazhi Liu, Xiang-qiang Chu, Marco Lagi, **Yang Zhang**, Emiliano Fratini, Piero Baglioni, Ahmet Alatas, Ayman Said, Ercan Alp and Sow-Hsin Chen, "Studies of phononlike low-energy excitations of protein molecules by inelastic X-ray scattering", Phys. Rev. Lett. 101, 135501 (2008).

- Selected on Virtual Journal of Nanoscale Science and Technology, Vol. 18, Issue 14 (2008).
- Selected on Virtual Journal of Biological Physics Research, Vol. 16, Issue 7 (2008).
- Highlighted on APS Science and Research, "A Quantum of Vibration in an Unexpected Place".
- "The atomic dance of proteins", Highlighted on APS Science 2008, 68-69 (2008).

[14] Sow-Hsin Chen, Francesco Mallamace, Li Liu, Dazhi Liu, Xiangqiang Chu, **Yang Zhang**, Chansoo Kim, Antonio Faraone, Chung -Yuan Mou, Emiliano Fratini, Piero Baglioni, A.I. Kolesnikov and Victoria Garcia-Sakai, "Dynamic crossover phenomenon in confined supercooled water and its relation to the existence of a liquid-liquid critical point in water", AIP Conference Proceedings: Complex Systems 982, 39-52, Eds: M. Tokuyama, I. Oppenheim, H. Nishiyama (2008).

[15] Dazhi Liu, **Yang Zhang**, Yun Liu, Jianlan Wu, Chia-Cheng Chen, Chung-Yuan Mou and Sow-Hsin Chen, "Density measurement of 1-D confined water by small angle neutron scattering method: pore size and hydration level dependences", J. of Phys. Chem. B 112, 4309-4312 (2008).

[16] Dazhi Liu, **Yang Zhang**, Chia-Cheng Chen, Chung-Yuan Mou, Peter H. Poole

and Sow-Hsin Chen, "Observation of the density minimum in deeply supercooled confined water", Proc. of Natl. Acad. of Sci., 104, 9570-9574 (2007).

- Highlighted on the cover of PNAS.
- Highlighted on Nature Nanotechnology, "Supercooled liquid: Water ways".
- Highlighted on the cover of Science News.
- Highlighted on Journalreview.org.
- Highlighted on X-Ray Group Virtual Journal Club.
- Highlighted on an interview of Prof Chung-Yuan Mou on ScienceWatch.com.
- Selected on Virtual Journal of Biological Physics Research, Vol. 14, Issue 1 (2007).
- "The density minimum in deeply supercooled confined water", Highlighted on 2007 Accomplishments and Opportunities, NIST Center for Neutron Research, 8-9 (2007).

[17] Sow-Hsin Chen, Li Liu, Xiangqiang Chu, **Yang Zhang**, Emiliano Fratini, Piero Baglioni, Antonio Faraone and Eugene Mamontov, "Experimental evidence of fragile-to-strong dynamic crossover in DNA hydration water", J. of Chem. Phys. 125, 171103 (2006).

- Selected on Virtual Journal of Biological Physics Research, November 15, 2006.
- "A mechanism for the onset of bioactivity in biomolecules", Highlighted on 2006 Accomplishments and Opportunities, NIST Center for Neutron Research, 32-33 (2006).

THIS PAGE INTENTIONALLY LEFT BLANK

Appendix B

Proof of Doctoral Thesis Defense

Massachusetts Institute of Technology
77 Massachusetts Avenue, Building 24–101
Cambridge, Massachusetts 02139–4307

Department of Nuclear Science and Engineering Doctoral Thesis Defense

Title: Neutron Scattering Investigations on the Unusual Phase Behavior of Water

Author: Yang Zhang

Thesis Supervisor: Professor Sow-Hsin Chen

Thesis Reader: Professor Sidney Yip

Thesis Committee Members:

Professor Bilge Yildiz

Professor H Eugene Stanley

Professor Pablo G Debenedetti

Professor David Chandler

Figure B-1: Proof of Doctoral Thesis Defense

Bibliography

[1] G Adam and J Gibbs. On the temperature dependence of cooperative relaxation properties in glass-forming liquids. *The Journal of Chemical Physics*, Jan 1965. 55

[2] Christiane Alba-Simionesco, Gilberte Dosseh, E Dumont, B Frick, B Geil, Denis Morineau, V Teboul, and Y Xia. Confinement of molecular liquids: Consequences on thermodynamic, static and dynamical properties of benzene and toluene. *Eur Phys J E*, 12(1):19–28, Jan 2003. 28

[3] C. Austen Angell. Supercooled water. *Annu Rev Phys Chem*, 34:593–630, Jan 1983. 13

[4] C. Austen Angell. Formation of glasses from liquids and biopolymers, Jan 1995. 15

[5] C. Austen Angell. Amorphous water. *Annu Rev Phys Chem*, 55:559–583, Jan 2004. 13, 14

[6] C. Austen Angell. Glass transition dynamics in water and other tetrahedral liquids: 'order-disorder' transitions versus 'normal' glass transitions, Jan 2007. 45

[7] C. Austen Angell. Highs and lows in the density of water, Jan 2007. 32

[8] C. Austen Angell. Glass-formers and viscous liquid slowdown since david turnbull: Enduring puzzles and new twists, Jan 2008. 15

[9] C. Austen Angell. Insights into phases of liquid water from study of its unusual glass-forming properties, Jan 2008. 15

[10] M. A Anisimov, J Sengers, and J Levelt Sengers. Near-critical behaviour of aqueous systems. *Aqueous Systems at Elevated Temperatures and Pressures: Physical Chemistry in Water, Steam and Hydrothermal Solutions*, Jan 2004. 21

[11] Philip Ball. *Life's Matrix: A Biography of Water*. Jan 2000. 13

[12] Philip Ball. Does hot water freeze first? *Phys World*, 19(4):19–21, Jan 2006. 14

[13] Philip Ball. Water: Water - an enduring mystery. *Nature*, 452(7185):291–292, Jan 2008. 13, 15

[14] D Banerjee, S. N Bhat, and D Leporini. Esr evidence for 2 coexisting liquid phases in deeply supercooled bulk water. *P Natl Acad Sci Usa*, 106(28):11448–11453, Jan 2009. 41

[15] JA Barker and D Henderson. What is liquid - understanding states of matter, Jan 1976. 13

[16] Marie-Claire Bellissent-Funel, Sow-Hsin Chen, and JM Zanotti. Single-particle dynamics of water-molecules in confined space. *Phys Rev E*, 51(5):4558–4569, Jan 1995. 57

[17] C Bennemann, C Donati, J Baschnagel, and Sharon C Glotzer. Growing range of correlated motion in a polymer melt on cooling towards the glass transition. *Nature*, 399(6733):246–249, Jan 1999. 55

[18] R Bergman and Jan Swenson. Dynamics of supercooled water in confined geometry. *Nature*, 403(6767):283–286, Jan 2000. 58

[19] L Berthier, Giulio Biroli, Jean-Philippe Bouchaud, Luca Cipelletti, D El Masri, D L'Hote, F Ladieu, and M Pierno. Direct experimental evidence of a growing length scale accompanying the glass transition. *Science*, 310(5755):1797–1800, Jan 2005. 56

[20] L Berthier, Giulio Biroli, Jean-Philippe Bouchaud, W Kob, Kunimasa Miyazaki, and David R Reichman. Spontaneous and induced dynamic correlations in glass formers. ii. model calculations and comparison to numerical simulations. *J Chem Phys*, 126(18):184504, Jan 2007. 56

[21] L Berthier, Giulio Biroli, Jean-Philippe Bouchaud, W Kob, Kunimasa Miyazaki, and David R Reichman. Spontaneous and induced dynamic fluctuations in glass formers. i. general results and dependence on ensemble and dynamics. *J Chem Phys*, 126(18):184503, Jan 2007. 56

[22] RJ Birgeneau, G Shirane, M Blume, and WC Koehler. Tricritical-point phase-diagram in fecl2. *Phys Rev Lett*, 33(18):1098–1101, Jan 1974. 45

[23] Jean Pierre Boon and Sidney Yip. *Molecular hydrodynamics*. Jan 1991. 16

[24] Ivan Brovchenko, A Geiger, and Alla Oleinikova. Multiple liquid-liquid transitions in supercooled water. *J Chem Phys*, 118(21):9473–9476, Jan 2003. 15

[25] Ivan Brovchenko, A Geiger, and Alla Oleinikova. Liquid-liquid phase transitions in supercooled water studied by computer simulations of various water models. *J Chem Phys*, 123(4):044515, Jan 2005. 15

[26] Ivan Brovchenko and Alla Oleinikova. Multiple phases of liquid water. *Chemphyschem*, 9(18):2660–2675, Jan 2008. 14, 15

[27] Sergey V Buldyrev, Pradeep Kumar, Pablo G Debenedetti, Peter J Rossky, and H. Eugene Stanley. Water-like solvation thermodynamics in a spherically symmetric solvent model with two characteristic lengths. *P Natl Acad Sci Usa*, 104(51):20177–20182, Jan 2007. 79

[28] Paul M. Chaikin and T C. Lubensky. *Principles of condensed matter physics.* Jan 2000. 20

[29] David Chandler. *Introduction to modern statistical mechanics.* Jan 1987. 20

[30] David Chandler. Hydrophobicity: Two faces of water. *Nature*, 417(6888):491–491, Jan 2002. 25

[31] David Chandler. Interfaces and the driving force of hydrophobic assembly. *Nature*, 437(7059):640–647, Jan 2005. 25

[32] Sow-Hsin Chen. Small-angle neutron-scattering studies of the structure and interaction in micellar and microemulsion systems. *Annu Rev Phys Chem*, 37:351–399, Jan 1986. 28

[33] Sow-Hsin Chen, P Gallo, Francesco Sciortino, and Piero Tartaglia. Molecular-dynamics study of incoherent quasielastic neutron-scattering spectra of supercooled water. *Phys Rev E*, 56(4):4231–4243, Jan 1997. 57

[34] Sow-Hsin Chen and Michael Kotlarchyk. *Interactions of photons and neutrons with matter.* Jan 2007. 16

[35] Sow-Hsin Chen, Marco Lagi, Xiang qiang Chu, Yang Zhang, Chansoo Kim, Antonio Faraone, Emiliano Fratini, and Piero Baglioni. Dynamics of a globular protein and its hydration water studied by neutron scattering and md simulations, Jan 2010. 24

[36] Sow-Hsin Chen, CY Liao, Francesco Sciortino, P Gallo, and Piero Tartaglia. Model for single-particle dynamics in supercooled water. *Phys Rev E*, 59(6):6708–6714, Jan 1999. 57

[37] Sow-Hsin Chen, Li Liu, Emiliano Fratini, Piero Baglioni, Antonio Faraone, and Eugene Mamontov. Observation of fragile-to-strong dynamic crossover in protein hydration water. *P Natl Acad Sci Usa*, 103(24):9012–9016, Jan 2006. 50, 68

[38] Sow-Hsin Chen, Li Liu, Xiang qiang Chu, Yang Zhang, Emiliano Fratini, P Baglioni, Antonio Faraone, and Eugene Mamontov. Experimental evidence of fragile-to-strong dynamic crossover in dna hydration water. *J Chem Phys*, 125(17):171103, Jan 2006. 24, 68

[39] Sow-Hsin Chen, J Rouch, Francesco Sciortino, and Piero Tartaglia. Static and dynamic properties of water-in-oil microemulsions near the critical and percolation points. *J Phys-Condens Mat*, 6(50):10855–10883, Jan 1994. 57

[40] Sow-Hsin Chen and J Teixeira. Structure and fractal dimension of protein-detergent complexes. *Phys Rev Lett*, 57(20):2583–2586, Jan 1986. 57

[41] Sow-Hsin Chen, Yang Zhang, Marco Lagi, S. H Chong, Piero Baglioni, and Francesco Mallamace. Evidence of dynamic crossover phenomena in water and other glass-forming liquids: experiments, md simulations and theory. *J Phys-Condens Mat*, 21(50):504102, Jan 2009. 24

[42] Sow-Hsin Chen, Yang Zhang, Marco Lagi, Xiang qiang Chu, Li Liu, Antonio Faraone, Emiliano Fratini, and Piero Baglioni. The dynamic response function chi(t)(q,t) of confined supercooled water and its relation to the dynamic crossover phenomenon. *Z Phys Chem*, 224(13):109–131, Jan 2010. 24

[43] S-H Chong, S-H Chen, and F Mallamace. A possible scenario for the fragile-to-strong dynamic crossover predicted by the extended mode-coupling theory for glass transition. *J Phys-Condens Mat*, 21(50):504101, Jan 2009. 79

[44] R de Debru and JJM Beenakker. Some thermodynamic considerations on properties of liquid 3he-4he mixtures. *Physica*, 27(2):219–&, Jan 1961. 45

[45] P Debenedetti. *Metastable liquids: concepts and principles.* Jan 1996. 14

[46] Pablo G Debenedetti. Supercooled and glassy water. *J Phys-Condens Mat*, 15(45):R1669–R1726, Jan 2003. 13, 22

[47] Pablo G Debenedetti and H. Eugene Stanley. Supercooled and glassy water. *Phys Today*, 56(6):40–46, Jan 2003. 13, 22

[48] Pablo G Debenedetti and FH Stilling. Supercooled liquids and the glass transition, Jan 2001. 15

[49] Jeppe C Dyre. Colloquium: The glass transition and elastic models of glass-forming liquids, Jan 2006. 15

[50] MD Ediger, C. Austen Angell, and Sidney R Nagel. Supercooled liquids and glasses, Jan 1996. 15

[51] P A. Egelstaff. *An introduction to the liquid state.* Jan 1994. 16

[52] JR Errington and Pablo G Debenedetti. Relationship between structural order and the anomalies of liquid water. *Nature*, 409(6818):318–321, Jan 2001. 14

[53] Antonio Faraone, Kao-Hsiang Liu, Chung-Yuan Mou, Yang Zhang, and Sow-Hsin Chen. Single particle dynamics of water confined in a hydrophobically modified mcm-41-s nanoporous matrix. *J Chem Phys*, 130(13):134512, Jan 2009. 24

[54] Antonio Faraone, Li Liu, and Sow-Hsin Chen. Model for the translation-rotation coupling of molecular motion in water. *J Chem Phys*, 119(12):6302–6313, Jan 2003. 57

[55] Antonio Faraone, Li Liu, Chung-Yuan Mou, PC Shih, John R. D Copley, and Sow-Hsin Chen. Translational and rotational dynamics of water in mesoporous silica materials: Mcm-41-s and mcm-48-s. *J Chem Phys*, 119(7):3963–3971, Jan 2003. 57

[56] JL Finney, A Hallbrucker, I Kohl, A. K Soper, and DT Bowron. Structures of high and low density amorphous ice by neutron diffraction. *Phys Rev Lett*, 88(22):225503, Jan 2002. 41

[57] M Fisher and B Widom. Decay of correlations in linear systems. *The Journal of Chemical Physics*, Jan 1969. 36

[58] F Franks. Protein stability: the value of 'old literature'. *Biophys Chem*, 96(2-3):117–127, Jan 2002. 50

[59] Giancarlo Franzese, G Malescio, A Skibinsky, Sergey V Buldyrev, and H. Eugene Stanley. Generic mechanism for generating a liquid-liquid phase transition. *Nature*, 409(6821):692–695, Jan 2001. 79

[60] Giancarlo Franzese and H. Eugene Stanley. The widom line of supercooled water, Jan 2007. 45, 79

[61] Giancarlo Franzese, Kevin Stokely, Xiang qiang Chu, Pradeep Kumar, Marco G Mazza, Sow-Hsin Chen, and H. Eugene Stanley. Pressure effects in supercooled water: comparison between a 2d model of water and experiments for surface water on a protein, Jan 2008. 37

[62] B Frick and B Richter. The microscopic basis of the glass-transition in polymers from neutron-scattering studies. *Science*, 267(5206):1939–1945, Jan 1995. 76

[63] D. A Fuentevilla and M. A Anisimov. Scaled equation of state for supercooled water near the liquid-liquid critical point. *Phys Rev Lett*, 97(19):195702, Jan 2006. 15

[64] P Gallo, M Rovere, and Sow-Hsin Chen. Dynamic crossover in supercooled confined water: Understanding bulk properties through confinement. *J Phys Chem Lett*, 1(4):729–733, Jan 2010. 25

[65] P Gallo, M Rovere, and E Spohr. Glass transition and layering effects in confined water: A computer simulation study. *J Chem Phys*, 113(24):11324–11335, Jan 2000. 28

[66] P Gallo, M Rovere, and E Spohr. Supercooled confined water and the mode coupling crossover temperature. *Phys Rev Lett*, 85(20):4317–4320, Jan 2000. 79

[67] P Gallo, Francesco Sciortino, Piero Tartaglia, and Sow-Hsin Chen. Slow dynamics of water molecules in supercooled states. *Phys Rev Lett*, 76(15):2730–2733, Jan 1996. 57

[68] Juan P Garrahan and David Chandler. Coarse-grained microscopic model of glass formers. *P Natl Acad Sci Usa*, 100(17):9710–9714, Jan 2003. 15

[69] LD Gelb, KE Gubbins, R Radhakrishnan, and M Sliwinska-Bartkowiak. Phase separation in confined systems, Jan 1999. 41

[70] Nicolas Giovambattista, C. Austen Angell, Francesco Sciortino, and H. Eugene Stanley. Glass-transition temperature of water: A simulation study. *Phys Rev Lett*, 93(4):047801, Jan 2004. 79

[71] Wolfgang Götze and MR Mayr. Evolution of vibrational excitations in glassy systems. *Phys Rev E*, 61(1):587–606, Jan 2000. 76

[72] E H Graf, D M Lee, and JD Reppy. Phase separation and superfluid transition in liquid he3-he4 mixtures, Jan 1967. 45

[73] T. S Grigera, V Martin-Mayor, G Parisi, and P Verrocchio. Phonon interpretation of the 'boson peak' in supercooled liquids. *Nature*, 422(6929):289–292, Jan 2003. 76

[74] Jean Pierre Hansen and Ian Ranald McDonald. *Theory of simple liquids*. Jan 2006. 20

[75] Lester O Hedges, Robert L Jack, Juan P Garrahan, and David Chandler. Dynamic order-disorder in atomistic models of structural glass formers. *Science*, 323(5919):1309–1313, Jan 2009. 15

[76] VB Henriques, N Guisoni, MA Barbosa, M Thielo, and MC Barbosa. Liquid polyamorphism and double criticality in a lattice gas model. *Mol Phys*, 103(21-23):3001–3007, Jan 2005. 45

[77] L Hong, B Begen, A Kisliuk, S Pawlus, M Paluch, and A. P Sokolov. Influence of pressure on quasielastic scattering in glasses: Relationship to the boson peak. *Phys Rev Lett*, 102(14):145502, Jan 2009. 76

[78] C Huang, K. T Wikfeldt, T Tokushima, D Nordlund, Y Harada, U Bergmann, M Niebuhr, T. M Weiss, Y Horikawa, M Leetmaa, M. P Ljungberg, O Takahashi, A Lenz, L Ojamae, A. P Lyubartsev, S Shin, L. G. M Pettersson, and A Nilsson. The inhomogeneous structure of water at ambient conditions. *P Natl Acad Sci Usa*, 106(36):15214–15218, Jan 2009. 41

[79] K Ito, CT Moynihan, and C. Austen Angell. Thermodynamic determination of fragility in liquids and a fragile-to-strong liquid transition in water. *Nature*, 398(6727):492–495, Jan 1999. 58

[80] HM Jennings. A model for the microstructure of calcium silicate hydrate in cement paste. *Cement Concrete Res*, 30(1):101–116, Jan 2000. 51

[81] G. P Johari, Elpidio Tombari, Giuseppe Salvetti, and Francesco Mallamace. Does water need a lambda-type transition? *J Chem Phys*, 130(12):126102, Jan 2009. 45

[82] W KAUZMANN. Some factors in the interpretation of protein denaturation. *Adv Protein Chem*, 14:1–63, Jan 1959. 50

[83] EC Kerr. Density of liquid he-4. *J Chem Phys*, 26(3):511–514, Jan 1957. 45

[84] Chae Un Kim, Buz Barstow, Mark W Tate, and Sol M Gruner. Evidence for liquid water during the high-density to low-density amorphous ice transition. *P Natl Acad Sci Usa*, 106(12):4596–4600, Jan 2009. 41

[85] SB Kim, J Ma, and MHW Chan. Phase-diagram of he-3-he-4 mixture in aerogel. *Phys Rev Lett*, 71(14):2268–2271, Jan 1993. 45

[86] Pradeep Kumar, Sergey V Buldyrev, S. R Becker, Peter H Poole, Francis W Starr, and H. Eugene Stanley. Relation between the widom line and the breakdown of the stokes-einstein relation in supercooled water. *P Natl Acad Sci Usa*, 104(23):9575–9579, Jan 2007. 79

[87] Pradeep Kumar, Giancarlo Franzese, and H. Eugene Stanley. Predictions of dynamic behavior under pressure for two scenarios to explain water anomalies. *Phys Rev Lett*, 100(10):105701, Jan 2008. 76

[88] Pradeep Kumar, Zhenyu Yan, Limei Xu, Marco G Mazza, Sergey V Buldyrev, Sow-Hsin Chen, S Sastry, and H. Eugene Stanley. Glass transition in biomolecules and the liquid-liquid critical point of water. *Phys Rev Lett*, 97(17):177802, Jan 2006. 15

[89] Marco Lagi, Xiang qiang Chu, Chansoo Kim, Francesco Mallamace, Piero Baglioni, and Sow-Hsin Chen. The low-temperature dynamic crossover phenomenon in protein hydration water: Simulations vs experiments. *J Phys Chem B*, 112(6):1571–1575, Jan 2008. 66, 68

[90] CY Liao, Francesco Sciortino, and Sow-Hsin Chen. Model for dynamics in supercooled water. *Phys Rev E*, 60(6):6776–6787, Jan 1999. 57

[91] JA Lipa, DR Swanson, JA Nissen, and TCP Chui. Heat-capacity and thermal relaxation of bulk helium very near the lambda point, Jan 1994. 45

[92] Dazhi Liu, Xiang qiang Chu, Marco Lagi, Yang Zhang, Emiliano Fratini, Piero Baglioni, Ahmet Alatas, Ayman Said, Ercan Alp, and Sow-Hsin Chen. Studies of phononlike low-energy excitations of protein molecules by inelastic x-ray scattering. *Phys Rev Lett*, 101(13):135501, Jan 2008. 15, 24

[93] Dazhi Liu, Yang Zhang, Chia-Cheng Chen, Chung-Yuan Mou, Peter H Poole, and Sow-Hsin Chen. Observation of the density minimum in deeply supercooled confined water. *P Natl Acad Sci Usa*, 104(23):9570–9574, Jan 2007. 24, 33

[94] Dazhi Liu, Yang Zhang, Yun Liu, Jianlan Wu, Chia-Cheng Chen, Chung-Yuan Mou, and Sow-Hsin Chen. Density measurement of 1-d confined water by small angle neutron scattering method: Pore size and hydration level dependences. *J Phys Chem B*, 112(14):4309–4312, Jan 2008. 24

[95] Li Liu, Sow-Hsin Chen, Antonio Faraone, Chun-Wan Yen, Chung-Yuan Mou, Alexander I Kolesnikov, Eugene Mamontov, and Juscelino B Leao. Quasielastic and inelastic neutron scattering investigation of fragile-to-strong crossover in deeply supercooled water confined in nanoporous silica matrices. *J Phys-Condens Mat*, 18(36):S2261–S2284, Jan 2006. 57

[96] Li Liu, Sow-Hsin Chen, Antonio Faraone, CW Yen, and Chung-Yuan Mou. Pressure dependence of fragile-to-strong transition and a possible second critical point in supercooled confined water. *Phys Rev Lett*, 95(11):117802, Jan 2005. 57

[97] Li Liu, Antonio Faraone, and Sow-Hsin Chen. Model for the rotational contribution to quasielastic neutron scattering spectra from supercooled water. *Phys Rev E*, 65(4):041506, Jan 2002. 57

[98] Li Liu, Antonio Faraone, Chung-Yuan Mou, CW Yen, and Sow-Hsin Chen. Slow dynamics of supercooled water confined in nanoporous silica materials. *J Phys-Condens Mat*, 16(45):S5403–S5436, Jan 2004. 57

[99] Thomas Loerting, W Schustereder, Katrin Winkel, CG Salzmann, I Kohl, and Erwin Mayer. Amorphous ice: Stepwise formation of very-high-density amorphous ice from low-density amorphous ice at 125 k. *Phys Rev Lett*, 96(2):025702, Jan 2006. 41

[100] Ralf Ludwig. Water: From clusters to the bulk. *Angew Chem Int Edit*, 40(10):1808–1827, Jan 2001. 13, 14, 15

[101] Ralf Ludwig. The puzzling properties of supercooled and glassy water. *Angew Chem Int Edit*, 45(21):3402–3405, Jan 2006. 15

[102] A Luzar and David Chandler. Hydrogen-bond kinetics in liquid water. *Nature*, 379(6560):55–57, Jan 1996. 68

[103] Ateeque Malani, K. G Ayappa, and Sohail Murad. Influence of hydrophilic surface specificity on the structural properties of confined water. *J Phys Chem B*, 113(42):13825–13839, Jan 2009. 25

[104] Francesco Mallamace, Carmelo Corsaro, Matteo Broccio, Caterina Branca, N Gonzalez-Segredo, Jeroen Spooren, Sow-Hsin Chen, and H. Eugene Stanley. Nmr evidence of a sharp change in a measure of local order in deeply supercooled confined water. *P Natl Acad Sci Usa*, 105(35):12725–12729, Jan 2008. 43

[105] Satoshi Maruyama, Kenji Wakabayashi, and Masaharu Oguni. Thermal properties of supercooled water confined within silica gel pores. *AIP Conference Proceedings*, 708:675, 2004. 79

[106] Paul F McMillan and H. Eugene Stanley. Fluid phases going supercritical, Jan 2010. 15

[107] O Mishima. Reversible 1st-order transition between 2 h2o amorphs at similar-to-0.2 gpa and similar-to-135-k. *J Chem Phys*, 100(8):5910–5912, Jan 1994. 41

[108] O Mishima. Relationship between melting and amorphization of ice. *Nature*, 384(6609):546–549, Jan 1996. 41

[109] O Mishima. Liquid-liquid critical point in heavy water. *Phys Rev Lett*, 85(2):334–336, Jan 2000. 45

[110] O Mishima, LD Calvert, and E Whalley. Melting ice-i at 77-k and 10-kbar - a new method of making amorphous solids. *Nature*, 310(5976):393–395, Jan 1984. 41

[111] O Mishima, LD Calvert, and E Whalley. An apparently 1st-order transition between 2 amorphous phases of ice induced by pressure. *Nature*, 314(6006):76–78, Jan 1985. 41

[112] O Mishima and H. Eugene Stanley. Decompression-induced melting of ice iv and the liquid-liquid transition in water. *Nature*, 392(6672):164–168, Jan 1998. 41

[113] O Mishima and H. Eugene Stanley. The relationship between liquid, supercooled and glassy water, Jan 1998. 13, 14, 15, 41

[114] O Mishima, K Takemura, and K Aoki. Visual observations of the amorphous-amorphous transition in h2o under pressure. *Science*, 254(5030):406–408, Jan 1991. 41

[115] Denis Morineau, R Guegan, YD Xia, and Christiane Alba-Simionesco. Structure of liquid and glassy methanol confined in cylindrical pores. *J Chem Phys*, 121(3):1466–1473, Jan 2004. 28

[116] T Nakayama, K Yakubo, and RL Orbach. Dynamical properties of fractal networks - scaling, numerical simulations, and physical realizations, Jan 1994. 76

[117] RJ Nelmes, JS Loveday, T Strassle, CL Bull, M Guthrie, G Hamel, and S Klotz. Annealed high-density amorphous ice under pressure. *Nat Phys*, 2(6):414–418, Jan 2006. 41

[118] JJ Niemela and RJ Donnelly. Density and thermal-expansion coefficient of liquid-he-4 from measurements of the dielectric-constant. *J Low Temp Phys*, 98(1-2):1–16, Jan 1995. 45

[119] Masaharu Oguni, Satoshi Maruyama, Kenji Wakabayashi, and Atsushi Nagoe. Glass transitions of ordinary and heavy water within silica-gel nanopores. *Chem-Asian J*, 2(4):514–520, Jan 2007. 79

[120] Akira Onuki. *Phase transition dynamics*. Jan 2003. 16

[121] RL Orbach. Dynamics of fractal networks. *Science*, 231(4740):814–819, Jan 1986. 76

[122] Albert C Pan, Juan P Garrahan, and David Chandler. Heterogeneity and growing length scales in the dynamics of kinetically constrained lattice gases in two dimensions. *Phys Rev E*, 72(4):041106, Jan 2005. 55

[123] D Paschek. How the liquid-liquid transition affects hydrophobic hydration in deeply supercooled water. *Phys Rev Lett*, 94(21):217802, Jan 2005. 15

[124] Peter H Poole, T Grande, C. Austen Angell, and PF McMillan. Polymorphic phase transitions in liquids and glasses, Jan 1997. 41

[125] Peter H Poole, I Saika-Voivod, and Francesco Sciortino. Density minimum and liquid-liquid phase transition. *J Phys-Condens Mat*, 17(43):L431–L437, Jan 2005. 32

[126] Peter H Poole, Francesco Sciortino, U Essmann, and H. Eugene Stanley. Phase-behavior of metastable water. *Nature*, 360(6402):324–328, Jan 1992. 15

[127] Maria Antonietta Ricci, Fabio Bruni, and Alessia Giuliani. "similarities" between confined and supercooled water. *Faraday Discuss*, 141:347–358, Jan 2009. 15

[128] Francesca Ridi, Paola Luciani, Emiliano Fratini, and Piero Baglioni. Water confined in cement pastes as a probe of cement microstructure evolution. *J Phys Chem B*, 113(10):3080–3087, Jan 2009. 51

[129] G Salvetti, E Tombari, L Mikheeva, and GP Johari. The endothermic effects during denaturation of lysozyme by temperature modulated calorimetry and an intermediate reaction equilibrium. *J Phys Chem B*, 106(23):6081–6087, Jan 2002. 66

[130] S Sastry, Pablo G Debenedetti, Francesco Sciortino, and H. Eugene Stanley. Singularity-free interpretation of the thermodynamics of supercooled water. *Phys Rev E*, 53(6):6144–6154, Jan 1996. 15

[131] W Schirmacher. Thermal conductivity of glassy materials and the "boson peak". *Europhys Lett*, 73(6):892–898, Jan 2006. 76

[132] W Schirmacher, G Diezemann, and C Ganter. Harmonic vibrational excitations in disordered solids and the "boson peak". *Phys Rev Lett*, 81(1):136–139, Jan 1998. 76

[133] W Schirmacher, G Ruocco, and T Scopigno. Acoustic attenuation in glasses and its relation with the boson peak. *Phys Rev Lett*, 98(2):025501, Jan 2007. 76

[134] Francesco Sciortino, L Fabbian, Sow-Hsin Chen, and Piero Tartaglia. Supercooled water and the kinetic glass transition .2. collective dynamics. *Phys Rev E*, 56(5):5397–5404, Jan 1997. 57

[135] Francesco Sciortino, P Gallo, Piero Tartaglia, and Sow-Hsin Chen. Supercooled water and the kinetic glass transition. *Phys Rev E*, 54(6):6331–6343, Jan 1996. 57

[136] Francesco Sciortino and Piero Tartaglia. Harmonic dynamics in supercooled liquids: The case of water. *Phys Rev Lett*, 78(12):2385–2388, Jan 1997. 57

[137] T Scopigno, G Ruocco, F Sette, and G Monaco. Is the fragility of a liquid embedded in the properties of its glass? *Science*, 302(5646):849–852, Jan 2003. 76

[138] F Sette, MH Krisch, C Masciovecchio, G Ruocco, and G Monaco. Dynamics of glasses and glass-forming liquids studied by inelastic x-ray scattering, Jan 1998. 76

[139] Hiroshi Shintani and Hajime Tanaka. Universal link between the boson peak and transverse phonons in glass. *Nature Materials*, 7(11):870–877, Jan 2008. 76

[140] KA Snyder and DP Bentz. Suspended hydration and loss of freezable water in cement pastes exposed to 90 *Cement Concrete Res*, 34(11):2045–2056, Jan 2004. 52

[141] A. K Soper. Structural transformations in amorphous ice and supercooled water and their relevance to the phase diagram of water, Jan 2008. 15

[142] AK Soper. The radial distribution functions of water and ice from 220 to 673 k and at pressures up to 400 mpa. *Chem Phys*, 258(2-3):121–137, Jan 2000. 14

[143] Harry Eugene Stanley. *Introduction to phase transitions and critical phenomena.* Jan 1987. 19, 20, 22

[144] Francis W Starr, C. Austen Angell, E La Nave, S Sastry, A Scala, Francesco Sciortino, and H. Eugene Stanley. Recent results on the connection between thermodynamics and dynamics in supercooled water. *Biophys Chem*, 105(2-3):573–583, Jan 2003. 79

[145] FH Stilling and TA Weber. Packing structures and transitions in liquids and solids. *Science*, 225(4666):983–989, Jan 1984. 15

[146] Jan Swenson, HM Janssen, and R Bergman. Relaxation processes in supercooled confined water and implications for protein dynamics. *Phys Rev Lett*, 96(24):247802, Jan 2006. 68

[147] Hajime Tanaka. A self-consistent phase diagram for supercooled water. *Nature*, 380(6572):328–330, Jan 1996. 45

[148] Hajime Tanaka, Takeshi Kawasaki, Hiroshi Shintani, and Keiji Watanabe. Critical-like behaviour of glass-forming liquids. *Nature Materials*, 9(4):324–331, Jan 2010. 79

[149] MM Teeter. Water-protein interactions - theory and experiment. *Annu Rev Biophys Bio*, 20:577–600, Jan 1991. 50

[150] J Teixeira, Marie-Claire Bellissent-Funel, Sow-Hsin Chen, and AJ Dianoux. Experimental-determination of the nature of diffusive motions of water-molecules at low-temperatures. *Phys Rev A*, 31(3):1913–1917, Jan 1985. 57

[151] PD Tennis and HM Jennings. A model for two types of calcium silicate hydrate in the microstructure of portland cement pastes. *Cement Concrete Res*, 30(6):855–863, Jan 2000. 51

[152] T Tokushima, Y Harada, O Takahashi, Y Senba, H Ohashi, L. G. M Pettersson, A Nilsson, and S Shin. High resolution x-ray emission spectroscopy of liquid water: The observation of two structural motifs, Jan 2008. 41

[153] C Toninelli, Matthieu Wyart, L Berthier, Giulio Biroli, and Jean-Philippe Bouchaud. Dynamical susceptibility of glass formers: Contrasting the predictions of theoretical scenarios. *Phys Rev E*, 71(4):041505, Jan 2005. 56

[154] CA Tulk, CJ Benmore, J Urquidi, DD Klug, J Neuefeind, B Tomberli, and PA Egelstaff. Structural studies of several distinct metastable forms of amorphous ice. *Science*, 297(5585):1320–1323, Jan 2002. 41

[155] V Velikov, S Borick, and C. Austen Angell. The glass transition of water, based on hyperquenching experiments. *Science*, 294(5550):2335–2338, Jan 2001. 79

[156] H Weintraub, M Ashburner, PN Goodfellow, HF Lodish, CJ Arntzen, PW Anderson, TM Rice, TH Geballe, AR Means, HM Ranney, TR Cech, RR Colwell, HR Bourne, B Richter, IM Singer, P Marrack, DT Fearon, A Penzias, AJ Bard, WF Brinkman, PA Marks, B Vogelstein, KW Kinzler, JM Bishop, RN Zare, G Schatz, SJ Benkovic, HB Gray, JS Valentine, PJ Crutzen, DW Choi, S Nakanishi, SM Kosslyn, JI Brauman, DC Rees, WJ Brill, J Schell, R Luhrmann, CL Will, W Wulf, GJ Vermeij, KJ Arrow, NJ Smelser, DL Anderson, and PH Abelson. Through the glass lightly. *Science*, 267(5204):1609–1618, Jan 1995. 49

[157] Katrin Winkel, Michael S Elsaesser, Erwin Mayer, and Thomas Loerting. Water polyamorphism: Reversibility and (dis)continuity. *J Chem Phys*, 128(4):044510, Jan 2008. 41

[158] Limei Xu, Pradeep Kumar, Sergey V Buldyrev, Sow-Hsin Chen, Peter H Poole, Francesco Sciortino, and H. Eugene Stanley. Relation between the widom line and the dynamic crossover in systems with a liquid-liquid phase transition. *P Natl Acad Sci Usa*, 102(46):16558–16562, Jan 2005. 36, 68, 79

[159] Limei Xu, Francesco Mallamace, Zhenyu Yan, Francis W Starr, Sergey V Buldyrev, and H. Eugene Stanley. Appearance of a fractional stokes-einstein relation in water and a structural interpretation of its onset. *Nat Phys*, 5(8):565–569, Jan 2009. 14

[160] Koji Yoshida, Toshio Yamaguchi, Shigeharu Kittaka, Marie-Claire Bellissent-Funel, and Peter Fouquet. Thermodynamic, structural, and dynamic properties of supercooled water confined in mesoporous mcm-41 studied with calorimetric, neutron diffraction, and neutron spin echo measurements. *J Chem Phys*, 129(5):054702, Jan 2008. 25

[161] YZ Yue and C. Austen Angell. Clarifying the glass-transition behaviour of water by comparison with hyperquenched inorganic glasses. *Nature*, 427(6976):717–720, Jan 2004. 79

[162] JM Zanotti, Marie-Claire Bellissent-Funel, and Sow-Hsin Chen. Relaxational dynamics of supercooled water in porous glass. *Phys Rev E*, 59(3):3084–3093, Jan 1999. 57

[163] Yang Zhang, Marco Lagi, Emiliano Fratini, Piero Baglioni, Eugene Mamontov, and Sow-Hsin Chen. Dynamic susceptibility of supercooled water and its relation to the dynamic crossover phenomenon. *Phys Rev E*, 79(4):040201, Jan 2009. 24, 50, 59, 60, 62, 63

[164] Yang Zhang, Marco Lagi, Dazhi Liu, Francesco Mallamace, Emiliano Fratini, Piero Baglioni, Eugene Mamontov, Mark Hagen, and Sow-Hsin Chen. Observation of high-temperature dynamic crossover in protein hydration water and its relation to reversible denaturation of lysozyme. *J Chem Phys*, 130(13):135101, Jan 2009. 24, 50, 67, 69, 70, 71, 73

[165] Yang Zhang, Marco Lagi, Francesca Ridi, Emiliano Fratini, P Baglioni, Eugene Mamontov, and Sow-Hsin Chen. Observation of dynamic crossover and dynamic heterogeneity in hydration water confined in aged cement paste. *J Phys-Condens Mat*, 20(13):502101, Jan 2008. 24, 50, 53

[166] Yang Zhang, Kao-Hsiang Liu, Marco Lagi, Dazhi Liu, Kenneth C Littrell, Chung-Yuan Mou, and Sow-Hsin Chen. Absence of the density minimum of supercooled water in hydrophobic confinement. *J Phys Chem B*, 113(15):5007–5010, Jan 2009. 24, 35, 37

Index